

SURGERY IN COLORED TENSOR MODELS

CARLOS I. PÉREZ-SÁNCHEZ

ABSTRACT. Rooted in group field theory and matrix models, random tensor models are a recent background-invariant approach to quantum gravity in arbitrary dimensions. Colored tensor models (CTM) generate random triangulated orientable (pseudo)-manifolds. We analyze, in low dimensions, which known spaces are triangulated by specific CTM interactions. As a tool, we develop the graph-encoded surgery that is compatible with the quantum-field-theory-structure and use it to prove that a single model, the complex φ^4 -interaction in rank-2, generates all orientable 2-bordisms, thus, in particular, also all orientable, closed surfaces. We show that certain quartic rank-3 CTM, the φ_3^4 -theory, has as boundary sector all closed, possibly disconnected, orientable surfaces. Hence all closed orientable surfaces are cobordant via manifolds generated by the φ_3^4 -theory.

Keywords: Random tensor models; Feynman diagrams; matrix models; quantum gravity.

CONTENTS

1. Introduction	2
2. Tensors models and their graph theory	4
2.1. Homology of colored graphs	6
2.2. Jackets and degree-computations	8
2.3. The boundary graph	10
2.4. The geometric realization of colored graphs	11
2.5. Ribbon and 3-colored graphs	12
3. Graph-encoded surgery	14
3.1. Colored graph surgery	14
3.2. Matrix models as tensor-models	16
4. Topological completeness of the boundary sector of the φ_3^4 -theory	19
5. Conclusions	23
Appendix A. Computing homology of colored graphs	26
Appendix B. The cell complex of a ribbon graph	27
References	30

1. INTRODUCTION

Colored tensor models (CTM) have recently flourished as a random-geometry framework that has proven the ability to model quantum gravity in arbitrary dimension D [1, 21, 38, 37], partially following the line of thought of the 2-dimensional quantum gravity modeled by random matrices [16]. CTMs are quantum field theories for rank- D tensors whose indices transform independently under given D representations of unitary groups in a very simple way (see below). The bridge to physics is, essentially,

$$\textit{Quantum} \rightarrow \textit{Random} \quad \text{and} \quad \textit{Gravity} \rightarrow \textit{Graph-encoded } D\text{-geometry}. \quad (1)$$

The Euclidean path integral formulation of CTM defines a measure that facilitates the first correspondence. The second ‘map’ is a simplicial version of the known General Relativity correspondence for $D \geq 2$, whose discrete analogue is the Regge action in terms of the deficit angles [7], here expressed in a graph-theoretical context. The Feynman graphs of colored tensor models have enough structure to encode a sensible space, thus, both correspondences in (1) harmonically coexist. A condensed summary for this framework is its ability to generate triangulations of (pseudo)manifolds¹ that can be averaged by using a Boltzmann weight, $\exp(-S)$, that a particular model’s classical action functional S determines.

In a historical vein, the term *color*, introduced by di Francesco [15], appeared first, as many conceptions in tensor models do, in the context in the theory of matrix models. In that setting colors stand for the different sizes of rectangular matrix fields. The idea that ‘coloring’ prevents certain indices from being summed (contracted) with each other was successfully carried on by Gurău [21], who introduced several ‘colored’ tensor fields, extending di Francesco’s idea to the context of Group Field Theories [18, 32] in order to exclude graphs that could not encode reasonable spaces. The additional tensor fields can be integrated out, thus obtaining an effective action for a single field (see e.g. [15, Sec. 5]), which, however, retains the colored structure.

Nowadays (*random*) *tensor models* stands for a rather boarder cluster of alike theories [42, 12, 11] with physically promising features. In particular, just as matrix models, they support a large- N ‘t Hooft’s expansion which is controlled by an integer called *Gurău’s degree* [24, 22] that replaces the genus in matrix models (see Rem. 2). Parallel to the fairly vivid study of the QFT-techniques of tensor models (e.g. renormalization [5, 19, 27, 33, 6, 11, 9]), a topology and geometry ‘quota’ —in the CTM-setting is encoded in graph theory— that leads us to a better understanding of the gravitational-modeling, also deserves attention. These topics for low dimensional scenarios is what this paper is all about.

At the core of the link between graph theory and geometry that concerns us lies *Pezzana’s theorem* [36] on manifold crystallization. It allows piecewise linear manifolds to be represented by decorated graphs, the so-called *colored graphs*. This family of graphs corresponds to the Feynman graphs of colored tensor models. Thus, after Gurău’s work [21, 23], Pezzana’s theorem yields a surjection

$$\{\textit{All rank-}D \textit{ tensor model actions } S_{\text{int}}\} \longrightarrow \{\textit{PL-}D\textit{-manifolds}\}.$$

What Pezzana’s theorem does not specify is the tensor-model action that generates the graphs that represent certain class of manifolds. In physics one commonly scrutinizes a single model. Therefore it is interesting to pose the following question:

$$\textit{Given a class of manifolds, which CTM-action generates it?} \quad (\star)$$

The action should be polynomial by physical reasons. Thus, given a family \mathcal{C} of manifolds (up to equivalence \sim), one wishes to find a tensor-model action S_{int} and to prove the surjectivity of

¹ Pseudomanifolds are simplicial complexes that are non branching, pure and strongly connected. Since we aim at the construction of actual PL-manifolds, we do not deepen in that concept. Moreover we work here in dimensions 2 and 3 and piecewise linear manifolds is all we need, by Moise’s theorem [29]. Thus, henceforth we only write ‘manifold’.

the composition

$$\{\text{Feynman diagrams of } S_{\text{int}}\} \hookrightarrow \{(D+1)\text{-colored graphs}\} \xrightarrow{\Delta} \mathcal{C}/\sim,$$

where Δ is a ‘manifold reconstruction’-scheme (see Sec. 2.4 and [17]). Techniques like the bubble-homology of graphs [21] assist in distinguishing spaces (see Sec. 2.1) and shall be used here.

We fix now the setting to answer (\star) in low dimensions, that is, we choose the right family member of tensor models². Since we want to prove the surjectivity of certain maps, the result is stronger if we keep the classes of graphs emerging in that framework at its minimum, which means a large-symmetry in the action. The right choice is the complex CTM, as exposed in Section 2.

Having chosen the setting, we choose now the potential S_{int} . We work with rank-2 and rank-3 tensor models and in both instances we take a quartic potentials (which due to their distinct underlying structures look somehow different).

Our strategy is mainly surgery: In certain categories of manifolds, by using surgery one is able to generate new spaces and readily compute some topological invariants of them from the properties of their parts. It is therefore desirable to have this in the context of graphs. The existent concept in the context of the graph theoretical representation of piecewise linear manifolds by Pezzana, Gagliardi, Ferri *et al.* [17]—to our knowledge the only available concept—unfortunately does not respect the QFT-structure of tensor models, as we show here (Sec. 3, Rem. 4). We develop a QFT-compatible and CTM-compatible surgery aiming at answering (\star) for dimension 2, going further also to dimension 3. We stress that the methods provided by the theory of crystallization do not care about the graphs being Feynman diagrams of certain model.

Concretely, we obtain the following: A well-defined 3-colored graph surgery (Definition 10 for the connected sum and in Theorem 5, creation of boundary components), which restricts to the set of Feynman graphs of a given model. Remark 4 explains the need of this operation. These concepts lead to the parametrization of all orientable 2-bordisms by the diagrammatics of certain quartic potential (Thm. 5) and, in particular, the generation of all closed, connected orientable surfaces from (vacuum graphs of) the rank-2 *quartic* potential (Lemma 4). This is stronger than the \mathbb{R} -matrix model case, since, say, the following graph



of the real quartic matrix model is forbidden in any complex rank-2 theory.

Working in one dimension higher, we lift the surgery of 3-colored graphs to an operation on open 4-colored graphs and use this operation to prove that:

- Boundary graphs of a certain quartic rank-3 model, the so-called φ_3^4 -theory, generate all closed, connected orientable surfaces. That is, those surfaces are null-bordant in the sense of the φ_3^4 -theory.
- More generally, any two compact, orientable closed, *possible disconnected* surfaces are 3-cobordant by (a space reconstructed from) certain *connected* φ_3^4 -Feynman graph (Thm. 8).

This article has the following structure. We motivate first, in Section 2, the study of colored graphs by introducing from scratch, albeit quite straightforwardly, colored tensor models. A rather lengthy introduction on the graph theoretical machinery shall be provided there. The reader which is familiar with CTM can skip that section. Examples there (which we do not

² The generation of graphs and their characteristics are dependent on the type, structure and field chosen of tensor model chosen, i.e. whether it is colored, or hybrid, as multi-orientable tensor models [43]; and the vector spaces where the tensors are defined can also over \mathbb{R} or \mathbb{C} .

skimp on) shall become useful later on, though. Sections 3 and 4 are the core, where we prove our claims above. The reader that does not feel familiar with graph-homology and/or ribbon graphs might find useful Appendices A and/or B, respectively.

2. TENSORS MODELS AND THEIR GRAPH THEORY

Colored tensor models are quantum field theories for tensorial objects specified by an integer D and by so-called *interaction vertices*. The integer $D \geq 2$ is the rank of tensors fields $\bar{\varphi}, \varphi : \mathcal{H}_1 \otimes \mathcal{H}_2 \otimes \dots \otimes \mathcal{H}_D \rightarrow \mathbb{C}$ on products of Hilbert spaces $\mathcal{H}_1, \dots, \mathcal{H}_D$ and the interaction vertices $\{\text{Tr}_{\mathcal{B}_\alpha}(\varphi, \bar{\varphi})\}_\alpha$ are determined by invariance under products of unitary groups $\mathcal{U}(\mathcal{H}_1) \times \mathcal{U}(\mathcal{H}_2) \times \dots \times \mathcal{U}(\mathcal{H}_D)$, as we explain next. Renormalization should care for a second selection-process of interaction vertices consisting in suppressing those traces $\text{Tr}_{\mathcal{B}}$ which render the theory non-renormalizable (see e.g. [27, Sec. 3.7] for a list of the vertices \mathcal{B} ; those we shall deal with here are renormalizable). Since the following discussion and definitions can be carried out without any effort to higher rank, for sake of concreteness we restrict ourselves to rank-3, thus considering tensors $\varphi, \bar{\varphi} : \mathcal{H}_1 \otimes \mathcal{H}_2 \otimes \mathcal{H}_3 \rightarrow \mathbb{C}$. We also assume for simplicity, that \mathcal{H}_c are large but finite dimensional.

For any integer $c = 1, 2, 3$, which one calls *color*, take a basis $\{\vartheta_c^a : a \in I_c\}$ of the dual of \mathcal{H}_c . Here each $I_c \subset \mathbb{Z}$ serves as an index set, which will be often left implicit. We let $\varphi =: \sum_{a_1, a_2, a_3} \varphi_{a_1 a_2 a_3} \vartheta_1^{a_1} \otimes \vartheta_2^{a_2} \otimes \vartheta_3^{a_3}$. Each color- c index a_c transforms independently under a change of basis of \mathcal{H}_c . The coordinates transform therefore under unitary elements $W^{(c)} \in \mathcal{U}(\mathcal{H}_c)$ like

$$\begin{aligned} \varphi'_{a_1 a_2 a_3} &= \sum_{b_1, b_2, b_3} W_{a_1 b_1}^{(1)} W_{a_2 b_2}^{(2)} W_{a_3 b_3}^{(3)} \varphi_{b_1 b_2 b_3}, \\ \bar{\varphi}'_{a_1 a_2 a_3} &= \sum_{b_1, b_2, b_3} \bar{W}_{a_1 b_1}^{(1)} \bar{W}_{a_2 b_2}^{(2)} \bar{W}_{a_3 b_3}^{(3)} \bar{\varphi}_{b_1 b_2 b_3}. \end{aligned}$$

We take as classical action only invariants under the group $\mathcal{U}(\mathcal{H}_1) \times \mathcal{U}(\mathcal{H}_2) \times \mathcal{U}(\mathcal{H}_3)$. The only quadratic invariant, $S_0[\varphi, \bar{\varphi}] = \text{Tr}_2(\varphi, \bar{\varphi}) := \sum_{a_1, a_2, a_3} \bar{\varphi}_{a_1 a_2 a_3} \varphi_{a_1 a_2 a_3}$ is understood as the kinetic term³. Higher order terms like

$$\text{Tr}_{\mathcal{V}_2}(\varphi, \bar{\varphi}) = \lambda \sum_{\mathbf{a}, \mathbf{b}, \mathbf{p}, \mathbf{q}} \bar{\varphi}_{q_1 q_2 q_3} \bar{\varphi}_{p_1 p_2 p_3} (\delta_{a_1 p_1} \delta_{b_1 q_1} \delta_{a_2 p_2} \delta_{b_2 p_2} \delta_{a_3 p_3} \delta_{b_3 q_3}) \varphi_{a_1 a_2 a_3} \varphi_{b_1 b_2 b_3} \quad (3)$$

are the interaction vertices appearing in $S_{\text{int}} = \sum_\alpha \text{Tr}_{\mathcal{B}_\alpha}(\varphi, \bar{\varphi})$. By Schur's Lemma the tensors in the trace can be contracted only with δ 's (or multiples thereof, which can be absorbed in the *coupling constant* λ). The explicit expression of each one of these $\text{Tr}_{\mathcal{B}_\alpha}$ has certain number (say k) of fields $\bar{\varphi}_{\mathbf{p}^1}, \dots, \bar{\varphi}_{\mathbf{p}^k}$, which are fully contracted with same number of fields $\varphi_{\mathbf{a}^1}, \dots, \varphi_{\mathbf{a}^k}$, where $\mathbf{p}^i = (p_1^i, p_2^i, p_3^i)$, $\mathbf{a}^i = (a_1^i, a_2^i, a_3^i) \in I_1 \times I_2 \times I_3$ for each $i = 1, \dots, k$.

Here it is handy, in order to avoid writing these long expressions, to represent these vertices using either *stranded* graphs or their *colored, bipartite* version. The former is obtained as follows: each invariant trace must contain $\varphi_{a_1 a_2 a_3}$ and the complex conjugate field $\bar{\varphi}_{p_1 p_2 p_3}$. We represent these graphically by associating to them a bunch of $D = 3$ white nodes with outgoing strands and a bunch of $D = 3$ dark nodes with incoming strands respectively:

$$\varphi_{a_1 a_2 a_3} \mapsto \begin{array}{c} \text{green} \nearrow \\ \text{red} \nearrow \\ \text{blue} \nearrow \\ \textcircled{1} \textcircled{2} \textcircled{3} \end{array} \quad \text{and} \quad \bar{\varphi}_{p_1 p_2 p_3} \mapsto \begin{array}{c} \text{blue} \searrow \\ \text{red} \searrow \\ \text{green} \searrow \\ \textcircled{3} \textcircled{2} \textcircled{1} \end{array} \quad (\text{reversed order}).$$

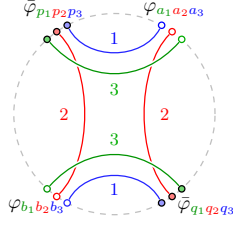
We associate to each δ single lines, in such a way that $\delta_{a_1 p_1} = \xrightarrow{1}$ connects the color-1 (green) strands of $\bar{\varphi}_{p_1 p_2 p_3}$ and $\varphi_{a_1 a_2 a_3}$; $\delta_{a_2 p_2} = \xrightarrow{2}$ connects the color-2 (red) strands and $\delta_{a_3 p_3} = \xrightarrow{3}$

³ In future work it will also consider a slightly modified trace with a symmetry-breaking term E , though:

$$S[\varphi, \bar{\varphi}] = \text{Tr}_2(\bar{\varphi}, E\varphi) + \sum_\alpha \text{Tr}_{\mathcal{B}_\alpha}(\varphi, \bar{\varphi}),$$

with $E : \mathcal{H}_1 \otimes \mathcal{H}_2 \otimes \mathcal{H}_3 \rightarrow \mathcal{H}_1 \otimes \mathcal{H}_2 \otimes \mathcal{H}_3$ 'self-adjoint', $\text{Tr}_2(\bar{\varphi}, E\varphi) = \text{Tr}_2(E\bar{\varphi}, \varphi)$. The first term is distinguished, and being quadratic in φ , it represents the kinetic part of the action, where E could be interpreted as the Laplacian. This allows to state Group Field Theories, via Fourier-transform, as colored tensor models.

those of color 3 (blue). Therefore the trace in eq. (3) is



It turns out that these graphs are still somehow quite elaborate and we will opt for even more simplified graphs that contain the same information. To the interactions one associates finite regularly edge-3-colored vertex-bipartite graphs. This picture is obtained from the stranded representation of graphs by collapsing the nodes $\circ \bullet \circ$ of $\varphi_{a_1 a_2 a_3}$ to a single white vertex \circ , and those of $\bar{\varphi}_{p_1 p_2 p_3}$, i.e. $\bullet \circ \bullet$, to a black vertex \bullet . Accordingly, the three strands of $\varphi_{a_1 a_2 a_3}$ join at \circ , and those of $\bar{\varphi}_{p_1 p_2 p_3}$ at \bullet , like

$$\varphi_{a_1 a_2 a_3} \mapsto \begin{array}{c} a_3 \\ \curvearrowright \\ \circ \\ \curvearrowleft \\ a_2 \end{array}, \quad \bar{\varphi}_{p_1 p_2 p_3} \mapsto \begin{array}{c} p_2 \\ \curvearrowright \\ \bullet \\ \curvearrowleft \\ p_3 \end{array}, \quad (4)$$

To the δ 's one associates numbered, or in the parlance *colored*, strands. Then the i -colored strand \xrightarrow{i} for $\delta_{a_i p_i}$ joins a_i and p_i in the vertices (4), so that, for instance eq. (3) becomes

$$\text{Tr} \gamma_2(\varphi, \bar{\varphi}) = \lambda \cdot \begin{array}{c} 3 \\ \circ \\ 1 \\ \circ \\ 1 \\ \bullet \\ 3 \end{array} \quad (5)$$

This completes the comments on notation of interaction vertices; now we address the corresponding notation of the Feynman graphs. The partition function reads⁴

$$Z[J, \bar{J}] = \frac{\int \mathcal{D}[\varphi, \bar{\varphi}] e^{\text{Tr}(\bar{J}\varphi) + \text{Tr}(\varphi J) - S[\varphi, \bar{\varphi}]}{\int \mathcal{D}[\varphi, \bar{\varphi}] e^{-S[\varphi, \bar{\varphi}]}} \quad \mathcal{D}[\varphi, \bar{\varphi}] := \prod_{\mathbf{a} \in I_1 \times I_2 \times I_3} \frac{d\varphi_{\mathbf{a}} d\bar{\varphi}_{\mathbf{a}}}{2\pi i}. \quad (6)$$

The quantity $d\mu(\varphi, \bar{\varphi}) = \mathcal{D}[\varphi, \bar{\varphi}] \exp(-S_0[\varphi, \bar{\varphi}])$ defines a Gaussian measure. Parenthetically, $d\mu$ and its perturbations, as other quantities can be formally studied in probability (see [25], where a tensor version of the Dyson-Wigner law is obtained) but that is beyond our aim in this paper.

The perturbative expansion yields the Wick's contraction of products of powers $[\text{Tr}_{\mathcal{B}_{\alpha_i}}(\varphi, \bar{\varphi})]^{n_i}$ of the interaction vertices, i.e. all different fully Wick-contracted terms obtained of the integrals of

$$[\text{Tr}_{\mathcal{B}_{\alpha_1}}(\varphi, \bar{\varphi})]^{n_1} [\text{Tr}_{\mathcal{B}_{\alpha_2}}(\varphi, \bar{\varphi})]^{n_2} \cdots [\text{Tr}_{\mathcal{B}_{\alpha_p}}(\varphi, \bar{\varphi})]^{n_p}, \quad (n_i \in \mathbb{Z}_{>0}).$$

The corresponding Feynman diagrams are $(3+1)$ -colored graphs (Sec. 2.1). It is illustrative to see how one arrives to that result departing from the stranded representation. First, we associate with the propagator that contracts a field φ with a $\bar{\varphi}$, three parallel colored dotted lines:

$$\begin{array}{c} \circ \text{---} \text{---} \text{---} \text{---} \bullet \\ \circ \text{---} \text{---} \text{---} \text{---} \bullet \\ \circ \text{---} \text{---} \text{---} \text{---} \bullet \end{array} = \begin{array}{c} 3 \circ \text{---} \text{---} \text{---} \bullet \\ 2 \circ \text{---} \text{---} \text{---} \bullet \\ 1 \circ \text{---} \text{---} \text{---} \bullet \end{array} \quad (7)$$

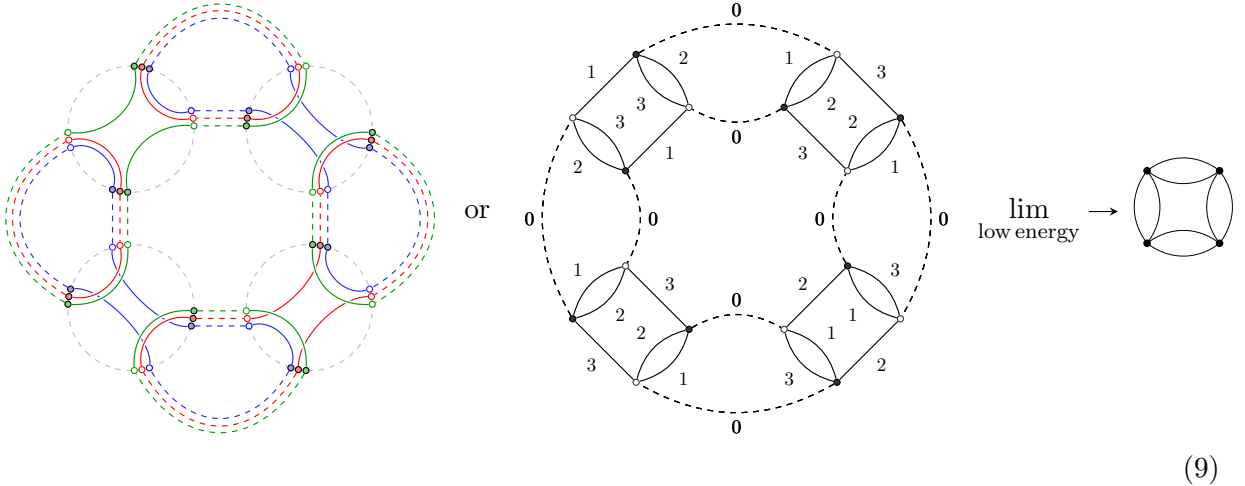
and the corresponding Wick's contraction, as usual in the CTM-literature, with the 0-color, $\circ \text{---} \text{---} \text{---} \bullet$, which is the simplified version of the stranded representation in eq. (7). In that

⁴ Actually the partition function has a factor N^{D-1} ($N = |I_a|$ for $a = 1, \dots, D$) in front of the action $S[\varphi, \bar{\varphi}]$ in a more realistic scenario for a rank- D model, and the measure should be rescaled accordingly. Here we work with the graph structure of the theory and thus the factor can be restored anytime. See Remark 2 below.

notation, a perturbative expansion in the *the* $(\varphi_{D=3}^4)$ -theory, whose action is defined by the sum of the vertices

$$\mathcal{V}_1 = \lambda \cdot \begin{array}{c} 2 \\ \circ \quad \circ \\ \text{3} \\ \text{3} \\ \circ \quad \circ \\ 2 \end{array}, \quad \mathcal{V}_2 = \lambda \cdot \begin{array}{c} 3 \\ \circ \quad \circ \\ \text{1} \\ \text{1} \\ \circ \quad \circ \\ 3 \end{array}, \quad \mathcal{V}_3 = \lambda \cdot \begin{array}{c} 1 \\ \circ \quad \circ \\ \text{2} \\ \text{2} \\ \circ \quad \circ \\ 1 \end{array}, \quad (8)$$

generates 4-colored bipartite regular graphs in colors $\{0, 1, 2, 3\}$ by Wick-contracting these vertices. Among the, say, fourth-order terms like $\int d\mu(\varphi, \bar{\varphi})(\mathcal{V}_1 \mathcal{V}_2 [\mathcal{V}_3]^2)$, the following is an example of vacuum graph contribution:



Both (big) graphs have the same information and are the ‘tensor-model’ version of the rightmost φ^4 -scalar field diagram, seen with higher energy resolution.

Remark 1. The representations above have a slightly deceiving terminology. The graph \mathcal{G} in the left of (9) is called *uncolored graph* [41, Sec. 1.3]; the graph in the right is denoted by $\mathcal{G}_{\text{color}}$ or \mathcal{G}_c and is the colored version of \mathcal{G} . These terminology is also well-explained in [5, Def. 1 and Fig. 5]. Sometimes, avoiding the stranded representation, \mathcal{G} is represented as \mathcal{G}_c with lines that are fainted if they are c -colored ($c \neq 0$), but we refrain from doing so. In the initial version of colored tensors a collection of D random tensors, rather than a single one as here, was considered. Then $D - 1$ of them were integrated out, and what one remains with is an ‘uncolored’ [8] tensor model with another (effective) action, which however, had still the colors encoded in their indices. The difference is that the geometric realization for $\mathcal{G}_{\text{color}}$ includes a *face* for each loop in 2 arbitrary colors—either $0c$ or cd , for $c, d = 1, \dots, D$ ($c \neq d$). For the uncolored version, one considers the loops of colors $0c$; the equivalence of notations, as in (9), explains why. We shall no longer use the stranded representation and prefer the ‘colored one’, for which, however, we drop the label in $\mathcal{G}_{\text{color}}$ and use directly \mathcal{G} instead.

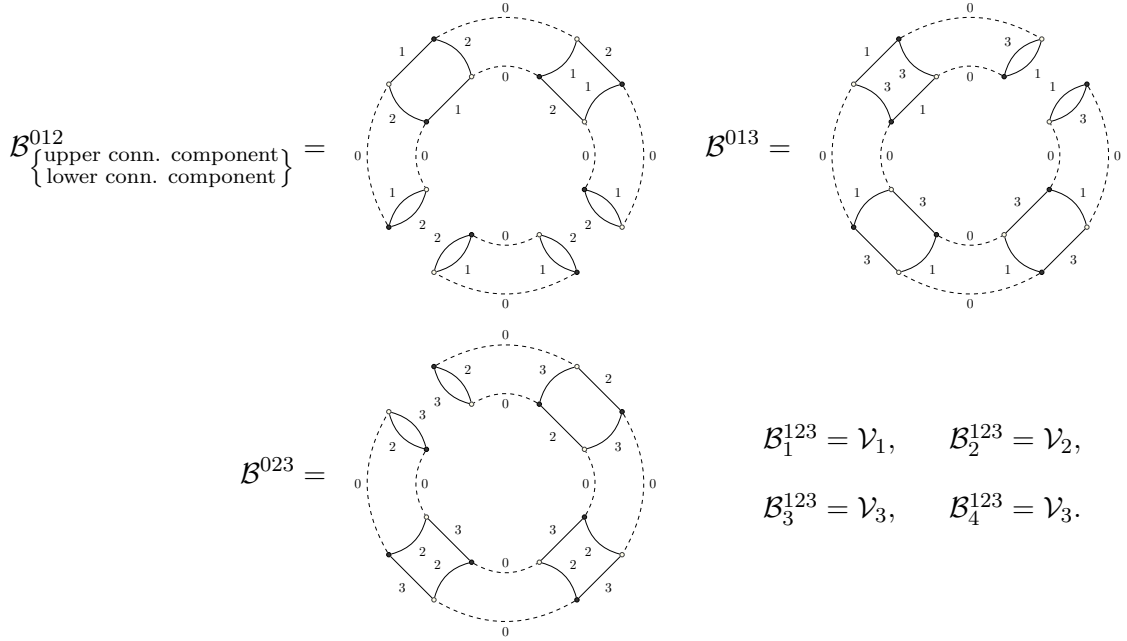
2.1. Homology of colored graphs.

Definition 1. By a D -colored graph, \mathcal{G} , one understands here a graph $\mathcal{G} = (\mathcal{G}^{(0)}, \mathcal{G}^{(1)})$ with the following properties:

- i) *Bipartiteness:* The *vertex set* is finite $\mathcal{G}^{(0)}$ and bipartite: $\mathcal{G}^{(0)} = \mathcal{G}_w^{(0)} \cup \mathcal{G}_b^{(0)}$, where $\mathcal{G}_w^{(0)}$ are the *white*, and $\mathcal{G}_b^{(0)}$ the *black* vertices. Further, any $e \in \mathcal{G}^{(1)}$ is attached to precisely one black vertex w and one white vertex, b , which we write $s(e) = b, t(e) = w$ or just $e = \bar{b}w$.
- ii) *Regular coloring:* The *edge set* is partitioned as $\mathcal{G}^{(1)} = \cup_{c=1}^D \mathcal{G}_c^{(1)}$. The elements of $\mathcal{G}_c^{(1)}$ are said to have color c ; this coloration is *regular*, i.e. there are D edges incident to any vertex having different colors.

We denote by $\text{Grph}_{\text{col},D}$ the set of connected D -colored graphs and by $\text{IIGrph}_{\text{col},D}$ the set of disconnected D -colored graphs. Graphs in either $\text{Grph}_{\text{col},D}$ or $\text{IIGrph}_{\text{col},D}$ are also called *closed*, in contrast to open graphs defined below (Sec. 2.3). A p -bubble \mathcal{B} of $\mathcal{G} \in \text{Grph}_{\text{col},D}$ is a connected subgraph of \mathcal{G} with edges in p fixed colors ($1 \leq p \leq D$), that is a subgraph \mathcal{B} of \mathcal{G} in $\text{Grph}_{\text{col},p}$ (the p colors being a subset of $\{1, \dots, D\}$). The set of p -bubbles of \mathcal{G} is denoted $\mathcal{G}^{(p)}$. This is consistent with $\mathcal{G}^{(0)}$ and $\mathcal{G}^{(1)}$ being the vertex and edge sets, respectively.

Example 1. Let \mathcal{G} be the Feynman graph (9). Then $\mathcal{G} \in \text{Grph}_{\text{col},3+1}$, \mathcal{G} having colors $\{0, 1, 2, 3\}$. The number of 0-bubbles (indexed by $\mathcal{G}^{(0)}$) is 16; it also has 32 1-bubbles, 8 of each color $c = 0, \dots, 3$ (indexed by $\mathcal{G}^{(1)}$); there are 24 2-bubbles sitting in \mathcal{G} : 3 bubbles of colors $\{01\}$ and $\{02\}$ each; 2 bubbles of colors $\{03\}$, 6 bubbles with colors $\{12\}$ and 5 with colors $\{13\}$ and $\{23\}$ each. The eight 3-bubbles are drawn here:



The theory of homology for the Feynman graphs of colored tensor models has been defined by Gurău [21] and, initially, it was referred to as *bubble-homology*. The term *colored homology* is also used. One defines the *chain complex* of the graph \mathcal{G} as the collection of groups $C_p(\mathcal{G}; \mathbb{Z}) = \text{span}_{\mathbb{Z}}\{\mathcal{B} \mid \mathcal{B} \text{ is a } p\text{-bubble of } \mathcal{G}\} = \text{span}_{\mathbb{Z}}(\mathcal{G}^{(p)})$ if $p = 0, \dots, D-1$, and $C_p(\mathcal{G}; \mathbb{Z}) = 0$ otherwise. (Hence, in the case of the example above $C_0(\mathcal{G}) = \mathbb{Z}^{16}$, $C_1(\mathcal{G}) = \mathbb{Z}^{32}$, $C_2(\mathcal{G}) = \mathbb{Z}^{24}$, $C_3(\mathcal{G}) = \mathbb{Z}^8$.) Any bubble in the generating set of $C_p(\mathcal{G}; \mathbb{Z})$ has then the form $\mathcal{B}_{\mathcal{V}}^I$ for $I \subset \{0, \dots, D\}$, $I = (i_1, \dots, i_p)$ fully ordered ($i_\alpha < i_\beta$ if $\alpha < \beta$) and \mathcal{V} some vertex or number determining the connected component. The *boundary map* is

$$\partial_p(\mathcal{B}_{\mathcal{V}}^{(i_1, \dots, i_p)}) = \sum_{q=1}^p (-1)^{q+1} \sum_{\mathcal{W} \subset \mathcal{V}} \mathcal{B}_{\mathcal{W}}^{i_1 \dots \widehat{i}_q \dots i_p} \quad \text{where } (p \geq 2).$$

The inner sum is performed over all the vertex-subsets \mathcal{W} of \mathcal{V} with colors $i_1 \dots \widehat{i}_q \dots i_p$. For arbitrary p one writes then:

$$\partial_p(\mathcal{B}_{\mathcal{V}}^{I^p}) = \begin{cases} 0 & \text{if } p = 0, \\ v - \bar{v} & \text{if } p = 1, \text{ and } \bar{v} = t(\mathcal{B}_{\mathcal{V}}^I), v = s(\mathcal{B}_{\mathcal{V}}^I) \\ \sum_{q=1}^p (-1)^{q+1} \sum_{\mathcal{W}_{\widehat{i}_q}} \mathcal{B}_{\mathcal{W}_{\widehat{i}_q}}^{i_1 \dots \widehat{i}_q \dots i_p} & \text{if } p \geq 2 \end{cases} \quad (10)$$

and the restriction to $\mathcal{W}_{\widehat{i}_q} \subset \mathcal{V}$ on the sum is implicit. Thus, one orients the edges e from the white (sources $s(e)$) into the black vertices (targets $t(e)$).

Definition 2. The *bubble homology* $H_*(\mathcal{G})$ of a colored graph \mathcal{G} is the homology of the chain complex $(C_*(\mathcal{G}), \partial_*)$. The *Euler characteristic* $\chi(\mathcal{G})$ of a colored graph \mathcal{G} is $\sum_q (-1)^q \text{rk} H_q(\mathcal{G})$.

Examples of the homology of graphs and the respective Euler characteristic follow. We also refer to Appendices A and B, for more detailed computations.

2.2. Jackets and degree-computations.

Definition 3. (Jackets and degree.) Let \mathcal{G} be a $(D + 1)$ -colored bipartite graph. Each cycle $\tau = (\ell_0 \dots \ell_D) \in \mathfrak{S}_{D+1}$, defines a graph \mathcal{J}_τ called *jacket* as follows: \mathcal{J}_τ has the same sets of vertices and edges as \mathcal{G} ,

$$\mathcal{J}_\tau^{(0)} := \mathcal{G}^{(0)}, \quad \mathcal{J}_\tau^{(1)} := \mathcal{G}^{(1)},$$

but its faces are those faces of \mathcal{G} (i.e. two-bubbles) that have colors $(\ell_{i+1}\ell_0)$ or $(\ell_i\ell_{i+1})$ with $i = 0, \dots, D$:

$$\mathcal{J}_\tau^{(2)} = \{f \in \mathcal{G}^{(2)} \mid f \text{ has colors } (\tau^q(0), \tau^{q+1}(0)), q \in \mathbb{Z}\}.$$

Here τ^q stands for $\tau \circ \dots \circ \tau$ applied (q times) to the color 0. By definition, $\mathcal{J}_\tau^{(k)} = \emptyset$ for $k > 2$, so that jackets are ribbon graphs. Since τ and τ^{-1} lead to the same face-sets, $\mathcal{J}_\tau^{(2)} = \mathcal{J}_{\tau^{-1}}^{(2)}$, those cycles are considered equivalent. Hence \mathcal{G} has $D!/2$ jackets. By computing their bubble-homology one finds, for certain non-negative integer $g_{\mathcal{J}}$,

$$H_q(\mathcal{J}) = \begin{cases} \mathbb{Z} & \text{if } q = 0, 2, \\ \mathbb{Z}^{2g_{\mathcal{J}}} & \text{if } q = 1, \\ 0 & \text{if } q > 2. \end{cases}$$

i.e. the Euler characteristic of the geometric realization of \mathcal{J} is $2 - 2g_{\mathcal{J}}$.

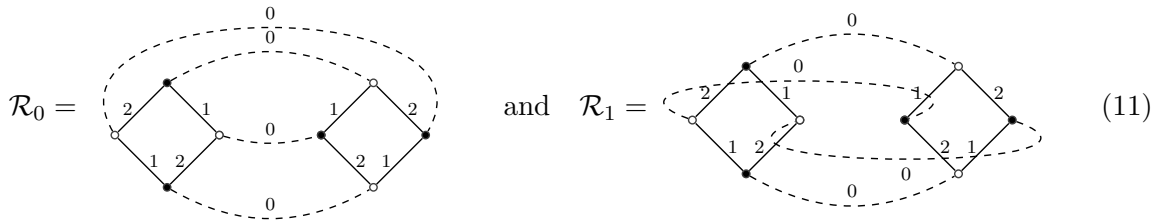
Definition 4. Given a closed graph $\mathcal{G} \in \text{Grph}_{\text{col}, D+1}$ ($D \geq 2$), its *Gurău's degree* $\omega(\mathcal{G})$ is defined as the sum of all the genera of the jackets of \mathcal{G} :

$$\omega(\mathcal{G}) = \sum_{\mathcal{J} \subset \mathcal{G}} g_{\mathcal{J}}.$$

A graph \mathcal{G} with $\omega(\mathcal{G}) = 0$ is called *melon*.

To fully understand the concept of jacket the next brief examples might help.

Example 2. The case $D = 2$. There, $(2 + 1)$ -colored graphs have a single jacket, the ribbon graph itself. The degree $\omega(\mathcal{R})$ is therefore precisely the genus $g(\mathcal{R})$. This will allow to treat matrix models as a rank-2 tensor model, as specified below 3.2. Consider the next graphs



arising in the $\mathcal{O}(\lambda^2)$ -terms from of the evaluation of the quartic rank-2 CTM,

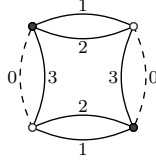
$$\int \mathcal{D}[\varphi, \bar{\varphi}] \exp(-\text{Tr}(\bar{\varphi}\varphi) - \lambda \text{Tr}((\bar{\varphi}\varphi)^2)),$$

where the 0-colored lines are Wick's contractions. The homology of \mathcal{R}_0 can be computed, but one can directly use its (dual) cell complex $\Delta(\mathcal{R}_0)$: the vertices and edges of the graph are the 0-cells and 1-cells of $\Delta(\mathcal{R}_0)$, respectively; to any bicolored path, one glues a 2-cell. Then $\Delta(\mathcal{R}_0)$ turns out to be a sphere. The graph \mathcal{R}_1 requires a slightly more detailed computation (see 9 in App. A). From its homology $H_0(\mathcal{R}_1) = \mathbb{Z}, H_1(\mathcal{R}_1) = \mathbb{Z}^2, H_2(\mathcal{R}_1) = \mathbb{Z}$, one infers that \mathcal{R}_1 is a (dual triangulation of a) torus.

Example 3. (When is a graph non-melonic?) There are at least four criteria to test non-melonicity:

- (i) Find a non-melonic subbubble $\mathcal{B}_{(\kappa_0)}^{\hat{D}}$ and use $\omega(\mathcal{G}) \geq D \sum_{\kappa} \omega(\mathcal{B}_{(\kappa)}^{\hat{D}})$ (see [25, Lemma 1] or [8, Prop. 2]), where κ indexes all 3-bubbles with colors \hat{D} .
- (ii) Since melonic graphs can be shown to be by necessity dual to spheres [24, Lemma 4], one can compute the homology $H_{\star}(\mathcal{G})$ and show that it is not isomorphic to the (say cell-) homology $H_{\star}^{\text{cell}}(\mathbb{S}^3)$ of a sphere.
- (iii) Find a non-spherical jacket of \mathcal{G} .
- (iv) Face-counting (cf. [8, Prop. 1] and [34]).

Contrary to matrix models, tensor models turn out to encode more than topology. That can be noted in the following example. Let \mathcal{G} be the following necklace-graph⁵ in four colors:



For this graph, (i) above does not help. Since all four 3-bubbles $\mathcal{B}^{\hat{0}}, \dots, \mathcal{B}^{\hat{3}}$ the same as the vertices \mathcal{V}_i . Thus those bubbles are melonic, and the lower bound given by (i) is trivially satisfied — by definition, $\omega(\mathcal{G})$ is already a non-negative integer. To begin with (ii) the chain complex is

$$0 \xrightarrow{\partial_4=0} C_3(\mathcal{G}) \simeq \mathbb{Z}^4 \xrightarrow{\partial_3} C_2(\mathcal{G}) \simeq \mathbb{Z}^8 \xrightarrow{\partial_2} C_1(\mathcal{G}) \simeq \mathbb{Z}^8 \xrightarrow{\partial_1} C_0(\mathcal{G}) \simeq \mathbb{Z}^4 \xrightarrow{\partial_0=0} 0.$$

Taking homology yields (see Ex. 10, App. A)

$$H_3(\mathcal{G}) = \mathbb{Z}, \quad H_2(\mathcal{G}) = 0, \quad H_1(\mathcal{G}) = 0, \quad H_0(\mathcal{G}) = \mathbb{Z}.$$

That method still does not help to know whether the graph is melonic, since \mathcal{G} has the same homology as \mathbb{S}^3 . Proceeding with (iii), one has for the jackets $\mathcal{J}_{\tau}, \mathcal{J}_{\pi}, \mathcal{J}_{\sigma}$ corresponding to $\tau = (0123), \pi = (0213), \sigma = (0132) \in \mathfrak{S}_4$, the following groups:

$$\begin{aligned} H_2(\mathcal{J}_{\tau}) &= \mathbb{Z}, & H_1(\mathcal{J}_{\tau}) &= 0, & H_0(\mathcal{J}_{\tau}) &= \mathbb{Z}, \\ H_2(\mathcal{J}_{\pi}) &= \mathbb{Z}, & H_1(\mathcal{J}_{\pi}) &= \mathbb{Z}^2, & H_0(\mathcal{J}_{\pi}) &= \mathbb{Z}, \\ H_2(\mathcal{J}_{\sigma}) &= \mathbb{Z}, & H_1(\mathcal{J}_{\sigma}) &= 0, & H_0(\mathcal{J}_{\sigma}) &= \mathbb{Z}. \end{aligned}$$

Therefore $\omega(\mathcal{G}) = 1$. Of course this is consistent with the face-counting formula [7, eq. 2.9] for d -colored graphs:

$$F_{\mathcal{G}} := \#(\mathcal{G}^{(2)}) = \binom{d-1}{2} \cdot \frac{\#(\mathcal{G}^{(0)})}{2} + (d-1) - \frac{2\omega(\mathcal{G})}{(d-2)!},$$

which in this case ($d = 3 + 1 = \#(\mathcal{G}^{(0)})$, $F_{\mathcal{G}} = 8$) also yields $\omega(\mathcal{G}) = 1$. By Proposition 4.3 of [26] (namely, four-colored graphs possessing a spherical jacket J , i.e. $g_J = 0$, are themselves spherical) one has a counterexample for the reciprocal of ‘being a melon implies being dual to a sphere’. In [39] it has been found that the jackets represent embedded matrix theories in the tensor theories. Moreover the jackets are interpreted as the surface along which a Heegaard splitting takes place. Here we found an example of this explicit splitting for the three-sphere. The genus-0 jackets \mathcal{J}_{τ} and \mathcal{J}_{σ} correspond to the genus-0 Heegaard splitting of $\mathbb{S}^3 \subset \mathbb{C}^2$, that is, the coordinates (z_1, z_2) of \mathbb{S}^3 with $\Im(z_2) = 0$, i.e. \mathbb{S}^2 inside \mathbb{S}^3 . The jacket \mathcal{J}_{π} is the genus-1 Heegaard splitting of \mathbb{S}^3 , the Clifford torus \mathbb{T}^2 , given by the locus $|z_1| = \sqrt{2}/2 = |z_2|$.

Remark 2. (On the importance of melons). So far we have considered the action functional as frozen, not flowing with the energy scale, N . This large integer is defined as follows. One usually sets the Hilbert spaces \mathcal{H}_c all to the fundamental representation of $U(N)$. One keeps

⁵The name ‘necklace’ has been borrowed from [10].

in mind the color as an artifact that forbids elements in one factor of $U(N) \times U(N) \times U(N)$ to jump to another one. The action (without sources) is then scaled as

$$Z_0 = \int \mathcal{D}[\varphi, \bar{\varphi}] e^{-N^{D-1} S[\varphi, \bar{\varphi}]} . \quad (12)$$

Melons are the dominating graphs, for the amplitude of a graph \mathcal{G} is weighted [23] by Gruău's degree as

$$\mathcal{A}(\mathcal{G}) \sim N^{D - \frac{2\omega(\mathcal{G})}{(D-1)!}} . \quad (13)$$

This is the tensor version of the well-known genus-weighted amplitudes of ribbon graphs \mathcal{R} in matrix models, $\mathcal{A}(\mathcal{R}) \sim N^{2-2g(\mathcal{R})}$. Having ribbon graphs a single jacket, the latter formula is a particular case of formula (13), with $D = 2$.

2.3. The boundary graph.

Definition 5. A graph \mathcal{G} is an *open* $(D + 1)$ -colored graph (with colors $c = 0, 1, \dots, D$) if its vertex-set is bipartite in the following two senses:

- (i) As before, $\mathcal{G}^{(0)} = \mathcal{G}_w^{(0)} \cup \mathcal{G}_b^{(0)}$, where $\mathcal{G}_w^{(0)}$ are the *white*, and $\mathcal{G}_b^{(0)}$ the *black* vertices,
- (ii) any vertex is either *inner* or *outer*, $\mathcal{G}^{(0)} = \mathcal{G}_{\text{inn}}^{(0)} \cup \mathcal{G}_{\text{out}}^{(0)}$; further, the set $\mathcal{G}_{\text{inn}}^{(0)}$ of inner vertices is regular with valence $D + 1$ and outer vertices have valence 1.

Additionally, the edge set $\mathcal{G}^{(1)}$ is $(D + 1)$ -colored —that is $\mathcal{G}^{(1)} = \cup_{c=0}^D \mathcal{G}_c^{(1)}$, where $\mathcal{G}_c^{(1)}$ is the set of color- c edges— and satisfies the following:

- (iii) for each color c and each inner vertex $v \in \mathcal{G}_{\text{inn}}^{(0)}$, there is exactly one color- c edge $e \in \mathcal{G}_c^{(1)}$ attached to v ,
- (iv) each external vertex is connected to the graph only by a color-0 edge.

Both the leaves of open graphs and the edges that are attached to them shall be referred to as *external legs*. Therefore alternative notations might include omission of the outer vertices ('half lines') or their replacement by sources. There, to each non-contracted black (resp. white) vertex, a (tensorial) source J (resp. \bar{J}) is attached). We also let

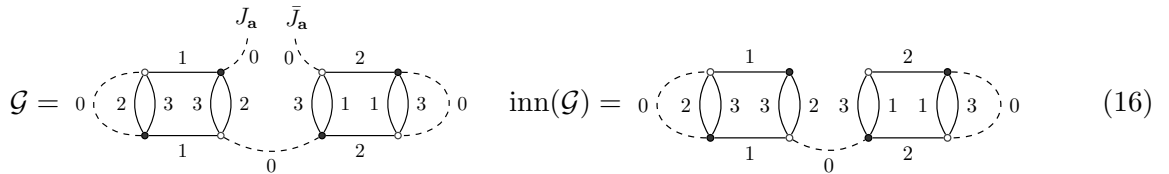
$$\text{Grph}_{\text{col}, D+1}^{(\mathcal{N})} := \{ \mathcal{G} \text{ open } (D + 1)\text{-colored} \mid \#(\mathcal{G}_{\text{out}}^{(0)}) = \mathcal{N} \} . \quad (14)$$

In the models we treat here, being the graphs bipartite, \mathcal{N} is even. We allow $\mathcal{N} = 0$, setting $\text{Grph}_{\text{col}, D+1}^{(0)} := \text{Grph}_{\text{col}, D+1}$. To complete the notation, given an open graph \mathcal{G} one can extract a (generally non-regularly) colored graph $\text{inn}(\mathcal{G})$ defined by

$$\text{inn}(\mathcal{G})^{(0)} = \mathcal{G}_{\text{inn}}^{(0)} \quad \text{inn}(\mathcal{G})^{(1)} = \mathcal{G}^{(1)} \setminus \{ \text{external legs of } \mathcal{G} \} . \quad (15)$$

The graph $\text{inn}(\mathcal{G})$ is called *amputated* graph.

For instance, the amputation of the the following open graph $\mathcal{G} \in \text{Grph}_{\text{col}, 3+1}^{(2)}$ is represented at its right-side:



In the QFT-context, open graphs are not-fully Wick-contracted interaction vertices.

Definition 6. A *colored tensor model* $V(\varphi, \bar{\varphi})$ is determined by an integer $D \geq 2$, called *dimension*, which is given by the rank of the tensors, and by an *action*

$$V(\varphi, \bar{\varphi}) = \sum_{\mathcal{B} \in \Upsilon} \lambda_{\mathcal{B}} \text{Tr}_{\mathcal{B}}(\varphi, \bar{\varphi}) ,$$

where $\Upsilon \subset \text{Grph}_{\text{col},D}$ is a finite subset and $\lambda_{\mathcal{B}} \in \mathbb{R}$ for each $\mathcal{B} \in \Upsilon$. The full action is then $S[\varphi, \bar{\varphi}] = \text{Tr}_2(\bar{\varphi}, \varphi) + V(\varphi, \bar{\varphi})$. The set of *connected Feynman diagrams* of the *model* $V(\varphi, \bar{\varphi})$ is denoted by $\mathfrak{Feyn}_D(V)$. It satisfies

$$\mathfrak{Feyn}_D(V) = \left\{ \mathcal{G} \in \cup_{k=0}^{\infty} \text{Grph}_{\text{col},D+1}^{(2k)} \mid \text{inn}(\mathcal{G})^{\hat{0}} \text{ has connected components in } \Upsilon \right\}.$$

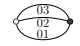
The graphs in $\text{Grph}_{\text{col},D+1}^{(0)} \cap \mathfrak{Feyn}_D(V) = \text{Grph}_{\text{col},D+1} \cap \mathfrak{Feyn}_D(V) := \mathfrak{Feyn}_D^{\text{vac}}(V)$ are called *vacuum graphs* of the model V . We write $\mathfrak{Feyn}_D^{\mathbb{R}}(V)$ if the tensor field is real.

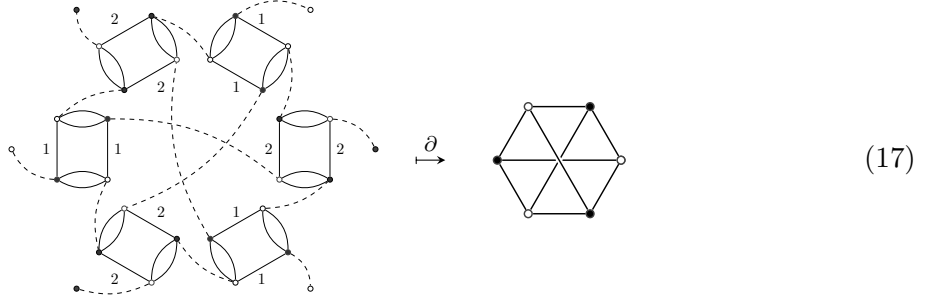
The boundary of a $(D + 1)$ -colored graph is a D -colored graph. It was defined in such a way that its associated (pseudo)simplicial complex matches the boundary of the complex of the original graph (see [26] for this fact). Thus, the boundary of a graph is defined to be empty on vacuum (i.e. closed) graphs. Otherwise:

Definition 7. Let \mathcal{G} be an open Feynman diagram of a rank- D colored tensor field theory. The *boundary graph* $\partial\mathcal{G}$ of \mathcal{G} has by definition the following vertex and edges sets:

$$(\partial\mathcal{G})^{(0)} = \mathcal{G}_{\text{out}}^{(0)}, \quad (\partial\mathcal{G})^{(1)} = \cup_{c=1}^D (\partial\mathcal{G})_c^{(1)}, \quad \text{with } (\partial\mathcal{G})_c^{(1)} = \{(0c)\text{-colored paths in } \mathcal{G}\}.$$

Another conventions define $(\partial\mathcal{G})^{(0)}$ as the set of external lines. Since an external line goes to an outer vertex, both definitions are equivalent. The definition also says that the outer vertices are the leaves of the graph. Two vertices of $\partial\mathcal{G}$ are connected by an i -colored edge if and only if there exists a $(0i)$ -bicolored path between them in \mathcal{G} .

Example 4. The graph \mathcal{G} in eq. (16) has two outer vertices, and by the previous construction, $\partial\mathcal{G}$ will have two vertices. For each $c = 1, 2, 3$, an edge of color c connects those, since there is a $(0c)$ -bicolored path between the two outer vertices \mathcal{G} . Then $\partial\mathcal{G}$ is  which does not differ (but apparently in labelling) from the graph of the propagator. A slightly more interesting example is



Boundary graph might be disconnected, as we will easily see (in Lemma 6, constructively).

2.4. The geometric realization of colored graphs. One can construct a colored triangulation $K(\mathcal{G})$ of a compact piecewise-linear manifold $|K(\mathcal{G})|$ departing from a $(D + 1)$ -colored graphs \mathcal{G} as we now describe. The simplicial (pseudo)complex $K(\mathcal{G})$ is assembled as follows [17]:

- for each $v \in \mathcal{G}^{(0)}$, $K(\mathcal{G})$ has a D -simplex σ_v
- one labels the vertices σ_v by the colors $\{0, 1, \dots, D\}$
- for each color c and each edge $e_c \in \mathcal{G}_c^{(1)}$ one identifies the faces $\sigma_{s(e_c)}$ and $\sigma_{t(e_c)}$ that do not contain the color c (i.e. the $(D - 1)$ -simplices that lie opposite to the vertex labelled by c)

Because colored graphs allow multiple edges, D -simplices might intersect at more than one face (whence the prefix *pseudo*). We write $|\Delta(\mathcal{G})|$ for the manifold that $K(\mathcal{G})$ triangulates, but we abuse on notation and abbreviate it as $\Delta(\mathcal{G})$. We say that \mathcal{G} *represents* $\Delta(\mathcal{G})$.

Remark 3. In the 2-dimensional case the cell complex associated to ribbon graphs and 3-colored graphs exposed in Appendix B is the Poincaré dual of this Δ -construct. Since we basically analyze the Euler characteristic of graphs, this subtlety is not important.

Colored graph theory also incarnates the cone $X \mapsto CX$ of a topological space [23]. If \mathcal{B} is a D -colored graph, then one defines $C\mathcal{B}$ as the open $(D+1)$ -colored graph with $(C\mathcal{B})_{\text{inn}}^{(0)} = \mathcal{B}^{(0)} \times \{0\}$ and $(C\mathcal{B})_{\text{out}}^{(0)} = \mathcal{B}^{(0)} \times \{1\}$ (a second copy of the vertices). Moreover, if $v \in \mathcal{B}^{(0)}$ is white (resp. black) then $(v, 0)$ is white (resp. black) as well, but $(v, 1)$ is black (resp. white). The edges are defined by

$$(C\mathcal{B})^{(1)} = \mathcal{B}^{(1)} \cup \{\text{single color-0 edge between } (v, 0) \text{ and } (v, 1) \mid v \in \mathcal{B}^{(0)}\}$$

The cone is defined so that $\Delta(C\mathcal{B}) = C\Delta(\mathcal{B})$. The relation $\partial(C\mathcal{B}) = \mathcal{B}$ holds also for each graph.

2.5. Ribbon and 3-colored graphs. Ribbon graphs are also known as *fat graphs*. We choose mainly the definition of [31] with a notation inspired by [30], but we will really need only a subset of those graphs, which arises either as Feynman diagrams in matrix models or as boundary-graphs of Feynman graphs of rank-3 tensor field theories. In all generality, though:

Definition 8. [30] A *ribbon graph* is a finite graph without isolated vertices nor leaves, together with a cyclic ordering of the set of half-edges at each vertex.

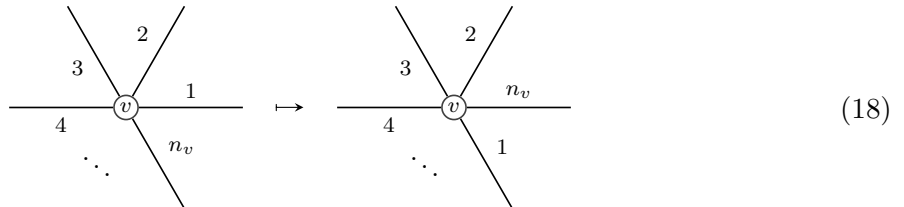
The definition includes [31], implicitly, the following set of data and conditions:

- two finite sets: the *vertex-set* $\mathcal{R}^{(0)}$, and the *half-edges* set $\mathcal{R}^{(1/2)}$.
- a map $p : \mathcal{R}^{(1/2)} \rightarrow \mathcal{R}^{(0)}$. The picture of ‘ $p(h) = v$ ’ is that the half-edge h emanates from v .
- $n_v := |p^{-1}(v)|$ is called the *valence* of a vertex v . Furthermore the condition $n_v > 1$ is imposed. Thus \mathcal{R} has neither isolated vertices ($n_v \neq 0$) nor leaves ($n_v \neq 1$).
- a cyclic orientation of $\mathcal{R}^{(1/2)}$.
- an involution j on the set of half-edges; here $j(h) = h'$ means that $\{h, h'\}$ is a full edge —if so then, of course, $j(h') = j^2(h) = h$. Moreover, it is imposed that j has no fixed point.

The usual graph notion in terms of vertices and (full) edges, $\mathcal{R} = (\mathcal{R}^{(0)}, \mathcal{R}^{(1)})$, is then recovered by defining $\mathcal{R}^{(1)}$, the *edge-set*, as the set of cycles of j [31]. Without loss of generality we write

$$\mathcal{R}^{(1/2)} = \{(v, \alpha) : v \in \mathcal{R}^{(0)}, \alpha = 1, \dots, n_v\} \quad \text{and} \quad p = \text{pr}_1.$$

Before formally constructing the cell-complex for a ribbon graph in Appendix B, we motivate in an informal vein their usual notation from the abstract definition. For a vertex $v \in \mathcal{R}^{(0)}$ of valence n_v , the cyclic ordering sees the following operation:



In order to keep track of the order, the incidence relations are usually graphically represented as follows: edges are *ribbons*, that is rectangles (topological disks D^2); vertices are *disks*. The map j represents the attachment of one side of a half-edge to a disk, as in Fig. 1 (A), thus keeping track of the operation (18). The cyclic ordering of the vertex determines an orientation on half-edges—rectangles as shown in Fig. 1 (B) and the ribbons should be drawn taking into account the orientation on both ends. Moreover, the ribbons do not intersect and the way they are attached to the disks must respect the orientation. If we represent the graph on the plane, mismatch of orientations is represented by lines \asymp , which do cross. Nevertheless, crucially,

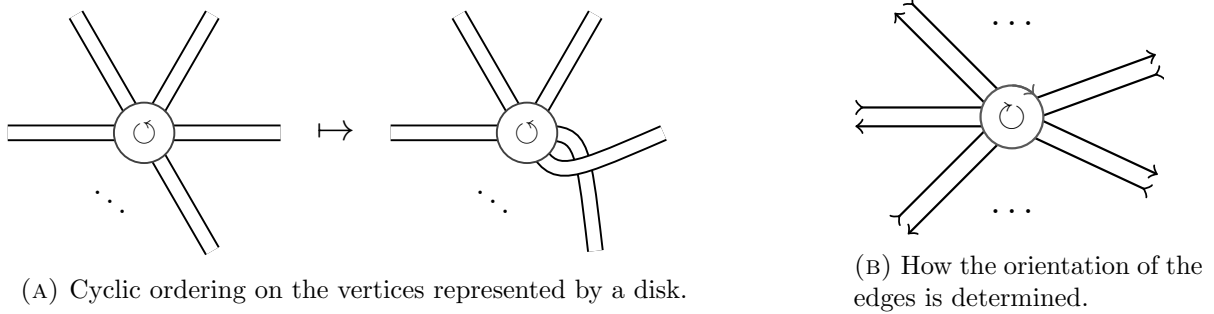


FIGURE 1

the graph can be drawn without intersections on other surfaces. The lowest-genus closed, orientable surface on a ribbon graph \mathcal{R} can be planarly drawn on is its geometric realization, $\Sigma(\mathcal{R})$ (see App. B for its construction).

Definition 9. We write $\chi(\mathcal{R})$ for the *Euler characteristic* of the geometric realization of \mathcal{R} , that is $\chi(\mathcal{R}) = \chi(\Sigma(\mathcal{R}))$. In turn, this also defines the *genus* $g(\mathcal{R})$ of \mathcal{R} .

Example 5. We illustrate the concepts in the last paragraph for the following simple ribbon graphs:

$$\mathcal{R} = \text{graph with two vertices and two edges}, \quad \mathcal{Q} = \text{graph with two vertices and two edges}, \quad \mathcal{W} = \text{graph with one vertex and two edges}.$$

Their ribbon representation is the following (thought of as filled vertices and ribbons):

$$\mathcal{R} = \text{fat graph with two vertices and two edges}, \quad \mathcal{Q} = \text{fat graph with two vertices and two edges}, \quad \mathcal{W} = \text{fat graph with one vertex and two edges}.$$

Thus, the fat graph \mathcal{R} has only one boundary component, so $\chi(\Sigma(\mathcal{R})) = 0$. Thus \mathcal{R} can only be planarly drawn on a torus. Also \mathcal{W} has genus 1, as it has only one boundary component, one vertex and two edges (ribbons). The graph \mathcal{Q} has genus 0. The notation we will choose from now on is the omission of the disks, usual in the physics literature, as well as disregarding crossings \asymp . With that notation, \mathcal{W} is shown in graph (2). This does not affect the previously defined quantities, because they are homotopy invariant.

Lemma 1. *Regularly edge-3-colored, vertex-bipartite graphs are ribbon graphs.*

Proof. Let $\mathcal{G} = (\mathcal{G}^{(0)}, \mathcal{G}^{(1)})$ be a 3-colored graph. We exhibit the ribbon graph structure of \mathcal{G} . The set of vertices of the ribbon graph is the same, $\mathcal{G}^{(0)}$. Define the set of half-edges $\mathcal{G}^{(1/2)} := \mathcal{G}^{(0)} \times \mathbb{Z}_3$, where $\mathbb{Z}_3 = \{1, 2, 3\}$. The map $p : \mathcal{G}^{(1/2)} \rightarrow \mathcal{G}^{(0)}$ is the projection $p = \text{pr}_1$, which satisfies $n_v > 1$ for each vertex $v \in \mathcal{G}^{(0)}$, since $p^{-1}(v) = \mathbb{Z}_3$. We let the cyclic order for white [resp. black] vertices be (123) [resp. (321)]. Finally, the involution j on $\mathcal{G}^{(1/2)}$ is defined as follows: given $h = (v, c) \in \mathcal{G}^{(1/2)}$, let $e \in \mathcal{G}^{(1)}$ be the edge of color c at v (because of regularity and coloring, e is uniquely determined) and w the other vertex e is attached to. Then let $j(h) := (w, c)$. The map j is an involution, since any two vertices can be connected only by one edge. \square

The converse of the previous lemma does not hold. For instance, consider the graph \mathcal{W} in Example 5 (or in 2). That ribbon graph is not bipartite, since it is a graph of a real model, $\mathcal{W} \in \mathfrak{Fen}_2^{\mathbb{R}}(\varphi^4)$. Regular colored bipartite graphs in more colors can be also given the structure of a ribbon graph, however the cell-attachment does not stop at dimension 2 (see App. B). This explains why having exactly 3 colors is important.

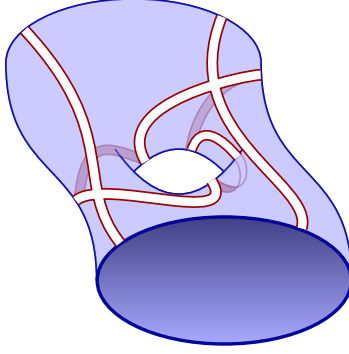


FIGURE 2. If one caps the two boundary components, one obtains \mathcal{R}_1 (Ex. 2)

3. GRAPH-ENCODED SURGERY

We develop elementary colored-graph-encoded surgery. The aim of this concept is twofold. The physical motivation is to see that we can expand the free energy $\log(Z[J, \bar{J}])$ of the model in sources indexed by ribbon graphs, having as goal the Ward Identity of the φ_3^4 -theory [35]. We will see here that this expansion is optimal after the identification of those ribbon boundary-graphs with closed, possibly disconnected Riemannian surfaces. The second aim, also for future work, is a macroscopic realization of the theory. This surgery shall become useful as for computing the space the final gluing of a large number of known ‘chunks of space’ represents.

An obstacle to perform this surgery is that one might have not enough simplices; in that case, by removing a simplex (or more), the space might fall apart into a topologically simpler one and information about its topology would be lost. In the same line of thought, there are subtleties concerning disk excision of open graphs (manifolds with boundary). With graphs, by doing what one could naively call ‘removing a disk’ \mathring{D}^n in the wrong place might not create a boundary component \mathbb{S}^{n-1} in the way one expects to do so. This phenomenon is better illustrated by example. Here, in the $\varphi_{D=2}^4$ (matrix)-theory, consider the graph \mathcal{R}_1 of Ex. 2. By cutting two color-0 edges one arrives to Figure 2, when one realizes it as a surface. But if one follows any of the two lines of the ‘boundary of the ribbon’ both connect the two boundary components of the surface.

3.1. Colored graph surgery. To prove our statements we need to see how to cut a 2-disk, in this realm, a two-bubble of a graph⁶.

Definition 10. Let \mathcal{R} and \mathcal{Q} be (closed) D -colored graphs, $\mathcal{R}, \mathcal{Q} \in \text{Grph}_{\text{col}, D}$. Let c be any color, and e and f be color- c edges in \mathcal{R} and \mathcal{Q} , respectively, i.e. $e \in \mathcal{R}_c^{(1)}$ and $f \in \mathcal{Q}_c^{(1)}$. We define the graph $\mathcal{R}_e \#_f \mathcal{Q}$ as follows:

$$(\mathcal{R}_e \#_f \mathcal{Q})^{(0)} = \mathcal{R}^{(0)} \cup \mathcal{Q}^{(0)} \quad \text{and} \quad (\mathcal{R}_e \#_f \mathcal{Q})^{(1)} = (\mathcal{R}^{(1)} \setminus \{e\}) \cup (\mathcal{Q}^{(1)} \setminus \{f\}) \cup \{e', f'\},$$

where e' and f' are c -colored edges defined by $s(e') = s(e)$, $t(e') = t(f)$ and $s(f') = s(f)$, $t(f') = t(e)$ (see Figure 3), which makes $\mathcal{R}_e \#_f \mathcal{Q}$ a connected graph in $\text{Grph}_{\text{col}, D}$. We will often obviate the edges and just write $\mathcal{R} \# \mathcal{Q}$ if this simplification does not lead to confusion.

⁶ For instance, take the surface in Figure 2 and put a cap in one of the boundary components (join one ribbon). If one takes two copies of this and tries to glue them along the boundary, and then represent this back as a colored graph, one arrives at definition 10

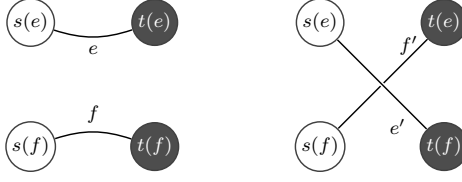


FIGURE 3. On Definition 10. Here s and t are source and target. The orientation of the edges is given by setting the ‘white vertices’ as sources.

Lemma 2. For any $\mathcal{R}, \mathcal{Q} \in \text{Grph}_{\text{col},3}$ and edges e in $\mathcal{R}_c^{(1)}$ and $f \in \mathcal{Q}_c^{(1)}$ of the same color c , the graph $\mathcal{R}_e \#_f \mathcal{Q} \in \text{Grph}_{\text{col},3}$ satisfies

$$\chi(\mathcal{R}_e \#_f \mathcal{Q}) = \chi(\mathcal{R}) + \chi(\mathcal{Q}) - 2.$$

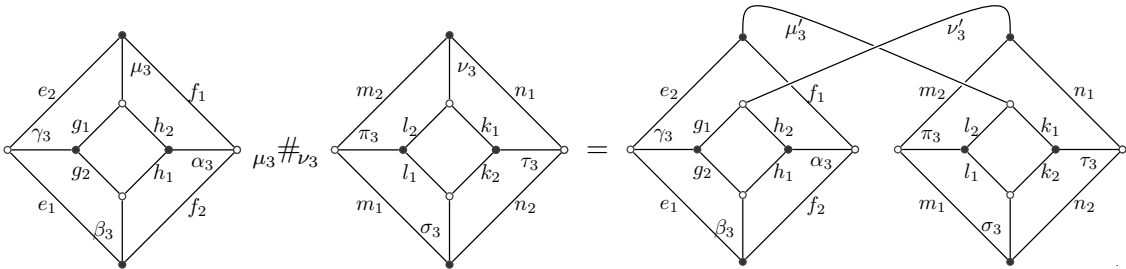
Proof. The operation $_e \#_f$ is additive with in vertices and edges. Thus, only the 2-bubbles might change:

$$\chi(\mathcal{R}_e \#_f \mathcal{Q}) = \chi(\mathcal{R}) + \chi(\mathcal{Q}) + (\text{created 2-bubbles} - \text{deleted 2-bubbles}).$$

Now, the change in the 2-bubbles can only take place in those containing the edges e or f . Since there are three colors, there are two 2-bubbles of \mathcal{R} , $\mathcal{B}_e^{cd}(\mathcal{R})$, containing e , namely those with colors (cd) , $d \in \{\hat{c}\}$. Similarly, there are two bubbles $\mathcal{B}_f^{cd}(\mathcal{Q})$ containing f . The removal of the edges e and f has as consequence the elimination of the 2-bubbles containing e and f , whence four 2-bubbles are eliminated in the new graph. Now, for each color $d \neq c$, the new edges e' and f' lie on the same 2-bubble of $\mathcal{R}_e \#_f \mathcal{Q}$. There is exactly one new bubble $\mathcal{B}_{e'f'}^{cd}(\mathcal{R}_e \#_f \mathcal{Q})$ for each d , thus 2 are created in total. Therefore the 2-bubbles decrease in two and the result follows. \square

The previous lemma justifies the notation in previous definition, since for compact, closed n -manifolds M and N one has $\chi(M \# N) = \chi(M) + \chi(N) - \chi(\mathbb{S}^n) = \chi(M) + \chi(N) + (-1)^{n+1} - 1$.

Example 6. We perform this first operation on the graphs for a torus and a sphere graphs, namely \mathcal{R}_0 and \mathcal{R}_1 of eq. (11), respectively:



Here each subindex of the edges corresponds with its coloring. Moreover, the color 0 has been replaced by 3, since the result holds for graphs in abstract (not only in the QFT context). According to the lemma, $\chi(\mathcal{R}_0 \# \mathcal{R}_1) = \chi(\mathcal{R}_0) + \chi(\mathcal{R}_1) - 2$. The same happens if we contract $\mathcal{R}_0 \# \mathcal{R}_1$ with another copy \mathcal{R}'_0 of \mathcal{R}_0 along the edges σ'_3 and β_3 , respectively. We get then $\Delta((\mathcal{R}_0 \# \mathcal{R}_1) \# \mathcal{R}'_0) \simeq \mathbb{T}^2$. This very graph will be used for the construction in Section 4.

Remark 4. If certain $(D + 1)$ -colored graph \mathcal{B} represents a (D) -dimensional manifold M one says that \mathcal{B} is a *crystallization* of M if moreover the number of D -bubbles in \mathcal{B} is exactly $D + 1$; or, rephrasing that condition, if by removing a single arbitrary color $i = 0, \dots, D$, one gets a connected graph \mathcal{B}^i . For example, the necklace graph in Example 3 is a crystallization, but the graph (9) is not.

The school of graph-theoretical representations of manifolds found a crystallization $\mathcal{B}_M \#_{\text{crys}} \mathcal{B}_N$ of the connected sum $M \# N$ two manifolds, from the crystallizations of \mathcal{B}_M and \mathcal{B}_N of the summands. In the orientable case (i.e. for bipartite graphs), in order to obtain $\mathcal{B}_M \#_{\text{crys}} \mathcal{B}_N$ one

deletes two vertices $p \in (\mathcal{B}_M)_w^{(0)}$ and $q \in (\mathcal{B}_N)_b^{(0)}$ and puts together, by color, the half-edges at $s^{-1}(p)$ and $t^{-1}(q)$ created by said vertex-removal.

If one wants to use directly $\#_{\text{crys}}$ a first issue is that crystallizations are not that abundant in $\mathfrak{Feyn}_D(V)$. Furthermore, the serious drawback is that one can always find Feynman diagrams \mathcal{B} and \mathcal{B}' of a model $V(\Phi)$, such that $\mathcal{B}\#_{\text{crys}}\mathcal{B}' \in \mathfrak{Feyn}_D(V)$ always lies outside the set of Feynman graphs $\mathfrak{Feyn}_D(V)$. Nothing forces $(\mathcal{B}\#_{\text{crys}}\mathcal{B}')^{\hat{0}}$ to be in the interaction potential V . Proposition 3 shows the advantage of using the operation $\#$ defined above instead. As a last reason to prefer $\#$ over $\#_{\text{crys}}$ is simplicity. Both are related by a 1-dipole insertion⁷:

$$\#_{\text{crys}} = (\text{1-dipole contraction}) \circ \# .$$

Although this relation can be inverted, it is $\#_{\text{crys}}$ which factors through a simpler operation, namely $\#$, and not the other way around. In the crystallization theory of manifolds it is understandable that $\#_{\text{crys}}$, which gets rid of two vertices, is natural, for it leads a colored graph towards a simpler one ('totally contracted', or properly a 'crystallization'). But here, precisely we do need those vertices to stay in the same model.

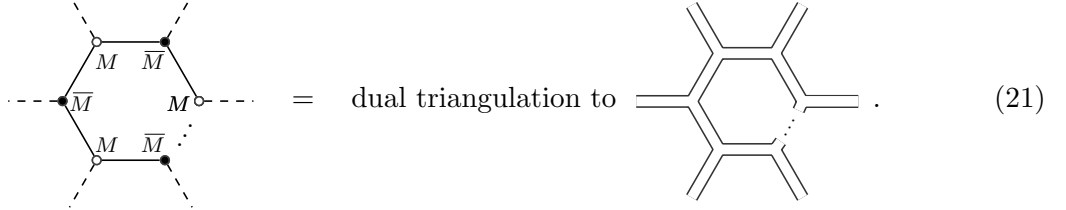
3.2. Matrix models as tensor-models. The perturbative expansion of the partition function of the matrix model

$$\int \mathcal{D}[M, \bar{M}] e^{-\text{Tr}(\bar{M}M) - \lambda V(M, \bar{M})} , \quad (19)$$

as is well-known, generates ribbon graphs, which are canonically given the structure of a triangulated surface by taking the dual complex of the construction $\Sigma(\mathcal{R})$ in Appendix B. Thus the interaction vertices of

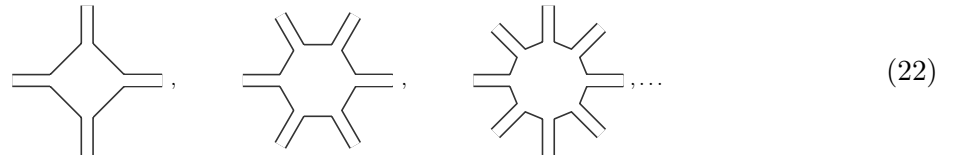
$$S[M, \bar{M}] = \text{Tr}(\bar{M}M) + V(M, \bar{M}) = \text{Tr}(\bar{M}M) + \lambda \text{Tr}((\bar{M}M)^p) \quad (20)$$

contribute with $(2p)$ -agonal vertices



$$= \text{dual triangulation to} \quad (21)$$

ribbon graph in the LHS is due to the construction in Lemma 1. We denote by $\mathfrak{Feyn}_2(\varphi^{2p})$ the set of Feynman diagrams of the theory defined by the functional (19). Other conventions differ from the one given so far. There, the loop inside the vertex, that is the (12)-colored bubble, is not drawn. For instance, if $p = 2, 3, 4$ one would have the following representation of the vertices:



$$, \quad (22)$$

that is, the colors $i = 1, 2$ are drawn as simple lines, and the 0-color double. The geometric realization is of course unaltered, since in the only difference is to decide whether one adds a vertex, as in the latter case (cf. (22)), or a face, as in the representation (21).

A (complex) matrix model here is, in the tensor model context, a polynomial interaction:

$$V(\varphi, \bar{\varphi}) = \sum_{p \in I} \lambda_p \text{Tr}((\varphi \bar{\varphi})^p) \quad (\text{finite } I \subset \mathbb{Z}_{>2}).$$

⁷The referee is acknowledged for this remark

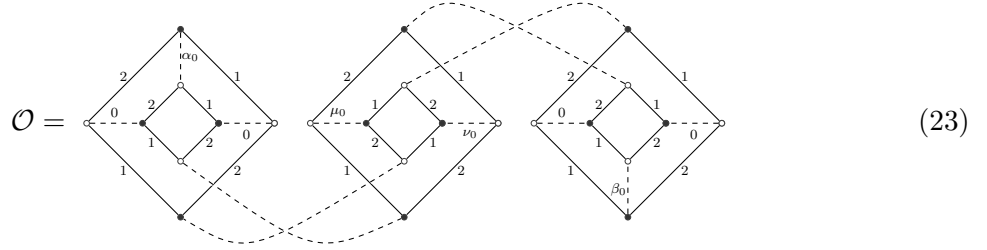
Proposition 3. Fix a rank-2 CTM (or a complex matrix model) interaction V . Let \mathcal{R} and \mathcal{Q} be Feynman diagrams of that model. Let $e \in \mathcal{R}_0^{(0)}$ and $f \in \mathcal{Q}_0^{(0)}$. Then $\mathcal{R}_e \#_f \mathcal{Q} \in \mathfrak{Feyn}_2(V)$ as well.

Proof. It is trivial by noticing that 0-colored edges are Wick contractions. \square

Let $\text{Riem}_{c,\text{cl},o}$ be the homeomorphism-classes of connected, closed orientable surfaces. We consider the empty surface also as an element of $\text{Riem}_{c,\text{cl},o}$. Then we claim that the only quartic model $\mathfrak{Feyn}_2^{\mathbb{C}}((\varphi\bar{\varphi})^2)$ has enough graphs to generate all of $\text{Riem}_{c,\text{cl},o}$. A weaker version of the following result corresponding to the real matrix φ^4 -theory might be known. In the complex theory with potential $(\varphi\bar{\varphi})^2$ some graphs of the real theory, $\mathfrak{Feyn}_2^{\mathbb{R}}(\varphi^4)$, are forbidden; nonetheless:

Lemma 4. There is a surjection $\mathfrak{Feyn}_2((\varphi\bar{\varphi})^2) \rightarrow \text{Riem}_{c,\text{cl},o}$.

Proof. Any vacuum graph \mathcal{G}_0 in $\text{Grph}_{\text{col},2+1}^{(0)} \subset \mathfrak{Feyn}_2^{\mathbb{C}}((\varphi\bar{\varphi})^2)$ yields the empty surface $\beta(\mathcal{G}_0) \in \text{Riem}_{c,\text{cl},o}$; we exclude this trivial case from now on. Because of the classification of orientable, closed surfaces, $\text{Riem}_{c,\text{cl},o} \simeq \mathbb{Z}_{\geq 0}$, one has to construct a graph for each $g \in \mathbb{Z}_{\geq 0}$. For $g = 0$, the graph \mathcal{R}_0 has been shown to triangulate \mathbb{S}^2 . For $g > 0$ we proceed differently. Let \mathcal{O} be the following graph:



Then consider g copies $\mathcal{O}^{(1)}, \dots, \mathcal{O}^{(g)}$, of that graph \mathcal{O} with distinguished 0-colored edges μ_0^i and ν_0^i , $i = 1, \dots, g$ as shown above. Then we claim that⁹

$$\mathcal{Q}_g := \mathcal{O}^{(1)} \#_{\mu_0^1 \#_{\nu_0^2} (\mathcal{O}^{(2)} \#_{\mu_0^2 \#_{\nu_0^3} (\mathcal{O}^{(3)} \#_{\mu_0^3 \#_{\nu_0^4} \dots \#_{\mu_0^{g-2} \#_{\nu_0^{g-1}} (\mathcal{O}^{(g-1)} \#_{\mu_0^{g-1} \#_{\nu_0^g} \mathcal{O}^{(g)}) \dots})} \dots) \quad (24)$$

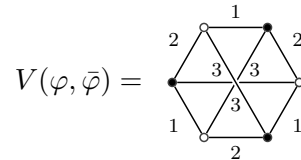
has genus g . Indeed, after Lemma 2 each sum $\#$ in (24) decreases the Euler characteristic in 2. Since each summand \mathcal{O} has $\chi(\mathcal{O}) = 0$ (cf. Example 6),

$$\chi(\mathcal{Q}_g) = (g-1) \cdot \chi(\mathcal{O}) - 2(g-1) = 2 - 2g.$$

\square

Remark 5. By the same token, one can also glue by α_0 and β_0 instead of by μ_0 and ν_0 . The resulting graph $\mathcal{K}_g := \mathcal{O}^{(1)} \#_{\beta_0^1 \#_{\alpha_0^2} (\mathcal{O}^{(2)} \#_{\beta_0^2 \#_{\alpha_0^3} (\dots \mathcal{O}^{(g-1)} \#_{\beta_0^{g-1} \#_{\alpha_0^g} \mathcal{O}^{(g)}) \dots})$ has genus g .

Example 7. In view of Lemma 4, the rank-3 model with interaction vertex set to \mathcal{Q}_g , for $g \geq 1$ (after properly changing the color 0 into 3), generates no melons at all. A lower-order polynomial interaction with the same characteristic is

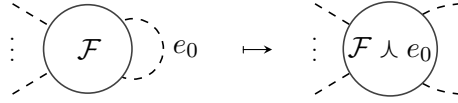


⁹ One can also do cell-counting: the number of vertices of this graph is $3 \cdot 8 \cdot g$; the number of edges is $3 \cdot 12 \cdot g$ and the number of faces is $|\mathcal{Q}_g^{(12)}| + |\mathcal{Q}_g^{(01)}| + |\mathcal{Q}_g^{(02)}| = 2 + 10 \cdot g$. Indeed, one sees trivially that the (12)-colored bubbles are $3 \cdot 2 \cdot g$. The only non-trivial part is to count the (0i)-bubbles. We see now by induction in the number g of sums $\#$ that the number of (01)-bubbles $|\mathcal{Q}_g^{(01)}|$ is $2g + 1$ and it is also evident that $|\mathcal{Q}_g^{(01)}| = |\mathcal{Q}_g^{(02)}|$.

This is consequence of the lower-bound for the degree (i), mentioned in example 3. Thus in rank-3 theories, an interaction vertex with suitable high degree (e.g. $g = 3$) has degree $\omega(\mathcal{G}) \geq 3$. Thus generation of spheres is not guaranteed (at least not before renormalization, if one does not introduce quadratic counterterms).

For any graph $\mathcal{F} \in \text{Grph}_{\text{col}, D+1}^{(2k)} \setminus \text{im } C$, i.e. for each graph \mathcal{F} that is not the cone of a D -colored graph, the set of inner propagators is not empty. For such graphs one can increase the number of external legs as follows:

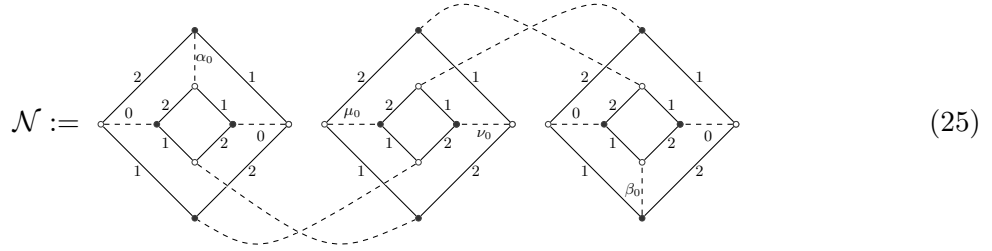
Definition 11. Let $k \in \mathbb{Z}_{\geq 0}$ and $\mathcal{F} \in \text{Grph}_{\text{col}, D+1}^{(2k)} \setminus \text{im } C$. Let $e_0 = (\overline{ap})$ an internal edge of \mathcal{F} . We denote by $\mathcal{F} \lambda e_0$ or $\mathcal{F} \lambda (\overline{ap})$ the graph obtained from \mathcal{F} by *opening* the 0-colored edge e_0 . By that, we mean that one creates two external legs (or leaves), one *at* a and one *at* p , so $\mathcal{F} \lambda e_0 \in \text{Grph}_{\text{col}, D+1}^{(2k+2)}$. Pictorially,



Theorem 5. Let 2-Cob be the set of all orientable 2-bordisms. There exists a surjection

$$\xi : \mathfrak{Feyn}_2((\varphi\bar{\varphi})^2) \rightarrow 2\text{-Cob}.$$

Proof. Consider the graph \mathcal{O} in (23) and let



Obviously, both graphs are in $\mathfrak{Feyn}_2((\varphi\bar{\varphi})^2)$. Let $M : \sqcup^C \mathbb{S}^1 \rightarrow \sqcup^B \mathbb{S}^1$ be an arbitrary element in 2-Cob . That is, two arbitrary closed 1-manifolds, $\sqcup^B \mathbb{S}^1$ and $\sqcup^C \mathbb{S}^1$ are cobordant via M , a genus- g orientable, compact surface with boundary. We now find a graph $\mathcal{Q}_{g,B,C}$ which (dually) triangulates M .

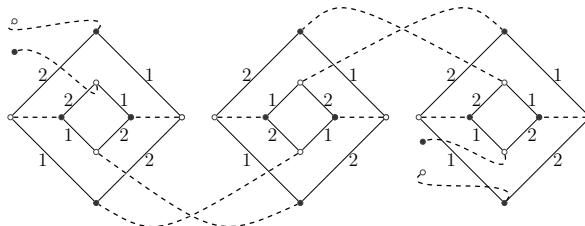
Remark that the case $B = C = 0$ is the statement in Lemma 4. Thus we can suppose $0 < B \leq C$ and set $m := \max\{g, C\} > 0$. Define the following Feynman-graph-valued functions:

$$\mathcal{X} : \{0, 1\} \rightarrow \mathfrak{Feyn}_2((\varphi\bar{\varphi})^2), \quad \mathcal{X}(\epsilon) = \begin{cases} \mathcal{N} & \text{if } \epsilon = 0, \\ \mathcal{O} & \text{if } \epsilon = 1, \end{cases}$$

and

$$\mathcal{S} : \{0, 1\} \times \{0, 1, 2\} \rightarrow \mathfrak{Feyn}_2((\varphi\bar{\varphi})^2), \quad \mathcal{S}(\epsilon, i) = \begin{cases} \mathcal{X}(\epsilon) & \text{if } i = 0, \\ \mathcal{X}(\epsilon) \lambda \alpha_0 & \text{if } i = 1, \\ (\mathcal{X}(\epsilon) \lambda \alpha_0) \lambda \beta_0 & \text{if } i = 2. \end{cases}$$

(For example, $\mathcal{S}(1, 2) = \mathcal{O} \lambda \alpha_0 \lambda \beta_0$, or explicitly,



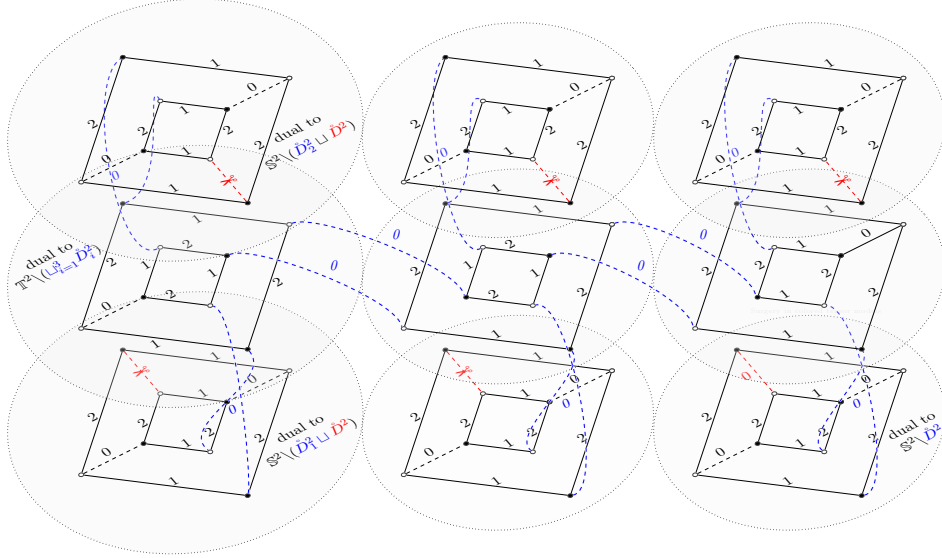


FIGURE 4. The triangulation of W given by the algorithm of Theorem 5

where the external lines come from cutting α_0 and β_0 .) Notice that the only difference between \mathcal{O} and \mathcal{N} is the edge-coloration of four edges, namely the central (12)-bicolored bubble adjacent to μ_0 and ν_0 . The following connected sum is well-defined:

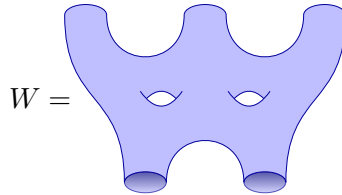
$$G((\epsilon_1, \iota_1), \dots, (\epsilon_m, \iota_m)) = \mathcal{S}(\epsilon_1, \iota_1) \#_{\mu_0^1 \# \nu_0^2} \mathcal{S}(\epsilon_2, \iota_2) \#_{\mu_0^2 \# \nu_0^3} \dots \#_{\mu_0^{m-1} \# \nu_0^m} \mathcal{S}(\epsilon_m, \iota_m),$$

where μ_0^i and ν_0^i refer, respectively, to the μ_0 and ν_0 edge of $\mathcal{X}(\epsilon_i)$. Define then the graph $\mathcal{Q}_{g,B,C}$ by evaluating $G((\epsilon_1, \iota_1), \dots, (\epsilon_m, \iota_m))$ at

$$\epsilon_k = \begin{cases} 1 & \text{if } 1 \leq k \leq g, \\ 0 & \text{if } k > g, \end{cases} \quad \text{and} \quad \iota_k = \begin{cases} 2 & \text{if } 1 \leq k \leq B, \\ 1 & \text{if } B < k \leq C, \\ 0 & \text{if } k > C. \end{cases}$$

Each 0-colored-edge removal creates exactly a boundary component \mathbb{S}^1 , for none of the 2-bubbles of α_0 and β_0 implies the edges μ_0 and ν_0 . Hence one has indeed created $C + B$ boundaries \mathbb{S}^1 . If we cap them (closing all the broken α_0 and β_0) we get $\mathcal{Q}_{g,0,0}$ which is the \mathcal{Q}_g of Lemma 4 and hence has genus g . \square

Example 8. Consider the following genus-2 bordism $W : \sqcup^3 \mathbb{S}^1 \rightarrow \sqcup^2 \mathbb{S}^1 \in 2\text{-Cob}$,



The construction for $\mathcal{Q}_{2,2,3}$ is, explicitly, the graph in Figure 4, in which we represented by \asymp the opening of the 0-colored edges. The theorem states that $\mathcal{Q}_{2,2,3} \in \mathfrak{Feyn}_2((\varphi\varphi^2))$ triangulates W .

4. TOPOLOGICAL COMPLETENESS OF THE BOUNDARY SECTOR OF THE φ_3^4 -THEORY

Let $\mathfrak{Feyn}_3(\varphi^4)$ be (shorthand for) the set of connected Feynman graphs of the rank-3 φ^4 -colored tensor theory with the three vertices in eq. (8). Throughout, $\text{Riem}_{c,cl,o}$ will be the set of homeomorphism-classes of closed orientable *connected* Riemannian surfaces, $\text{Riem}_{c,cl,o} \simeq \mathbb{Z}_{\geq 0}$. Further, we denote by $\text{Riem}_{cl,o}$ be the set of possibly disconnected closed, orientable Riemannian surfaces. In order to prove the main result of this section, we need.

It is trivial to construct Feynman graphs \mathcal{G} which have disconnected boundary, just by letting \mathcal{G} itself be disconnected. This would be rather useless, though, for \mathcal{G} would be cancelled out in the generating functional of connected correlation functions. The previous lemma says that, nevertheless, it is possible to ‘separate boundaries’ at wish. Moreover, it tells us how to generate *connected* graphs with a precise disconnected boundary.

Lemma 6. *The following two graphs $\mathcal{M}, \mathcal{P} \in \mathfrak{Feyn}_3(\varphi^4)$ separate boundary components:*

$$\mathcal{M} := m \quad \begin{array}{c} \text{2} \\ \text{1} \text{---} \text{3} \text{---} \text{2} \\ \text{3} \text{---} \text{1} \text{---} \text{3} \\ \text{2} \end{array} \quad \begin{array}{c} \text{0} \\ \text{1} \text{---} \text{2} \text{---} \text{1} \\ \text{2} \text{---} \text{3} \text{---} \text{2} \\ \text{0} \end{array} \quad \begin{array}{c} \text{3} \\ \text{1} \text{---} \text{2} \text{---} \text{1} \\ \text{2} \text{---} \text{3} \text{---} \text{2} \\ \text{0} \end{array} \quad \begin{array}{c} \text{1} \\ \text{2} \text{---} \text{3} \text{---} \text{2} \\ \text{3} \text{---} \text{1} \text{---} \text{3} \\ \text{1} \end{array} \quad n \quad \mathcal{P} := k \quad \begin{array}{c} \text{1} \\ \text{2} \text{---} \text{3} \text{---} \text{2} \\ \text{3} \text{---} \text{1} \text{---} \text{3} \\ \text{1} \end{array} \quad \begin{array}{c} \text{0} \\ \text{2} \text{---} \text{3} \text{---} \text{2} \\ \text{3} \text{---} \text{1} \text{---} \text{3} \\ \text{0} \end{array} \quad \begin{array}{c} \text{2} \\ \text{1} \text{---} \text{3} \text{---} \text{2} \\ \text{3} \text{---} \text{1} \text{---} \text{3} \\ \text{2} \end{array} \quad l \quad (26)$$

This means that, if \mathcal{G} and \mathcal{H} are φ_3^4 -Feynman graphs that are not in the image $\text{im } C$ of the cone, $\mathcal{G}, \mathcal{H} \in \mathfrak{Feyn}_3(\varphi^4) \setminus \text{im } C$, and g and h are internal propagators of \mathcal{G} and \mathcal{H} , respectively, then one has:

$$\partial(\mathcal{G}_g \#_k \mathcal{P}_l \#_h \mathcal{H}) = \partial\mathcal{G} \sqcup \partial\mathcal{H} \quad \text{and} \quad \partial(\mathcal{G}_g \#_m \mathcal{M}_n \#_h \mathcal{H}) = \partial\mathcal{G} \sqcup \partial\mathcal{H}. \quad (27)$$

We abbreviate $\mathcal{G}_g \#_k \mathcal{P}_l \#_h \mathcal{H}$ as $\mathcal{G} \# \mathcal{P} \# \mathcal{H}$ and choose a similar simplification for the other graph. Both $\mathcal{G} \# \mathcal{P} \# \mathcal{H}$ and $\mathcal{G} \# \mathcal{M} \# \mathcal{H}$ are in $\mathfrak{Feyn}_3(\varphi^4)$.

We do the proof for the equality in which \mathcal{P} occurs in one of the summands (by replacement of \mathcal{P} by \mathcal{M} one can get *mutatis mutandis* readily a proof). If \mathcal{Y} denotes $\mathcal{G} \# \mathcal{P} \# \mathcal{H}$ then Lemma 6 can be easily grasped as follows:

$$\partial\mathcal{Y} = \partial \left(\begin{array}{c} \text{---} \text{---} \text{---} \\ \text{---} \text{---} \text{---} \\ \text{---} \text{---} \text{---} \\ \text{---} \text{---} \text{---} \\ \text{---} \text{---} \text{---} \end{array} \right) = \partial \left(\begin{array}{c} \text{---} \text{---} \text{---} \\ \text{---} \text{---} \text{---} \\ \text{---} \text{---} \text{---} \\ \text{---} \text{---} \text{---} \\ \text{---} \text{---} \text{---} \end{array} \right) \sqcup \partial \left(\begin{array}{c} \text{---} \text{---} \text{---} \\ \text{---} \text{---} \text{---} \\ \text{---} \text{---} \text{---} \\ \text{---} \text{---} \text{---} \\ \text{---} \text{---} \text{---} \end{array} \right) = \partial\mathcal{G} \sqcup \partial\mathcal{H}.$$

Proof. It is obvious that \mathcal{Y} is in $\mathfrak{Feyn}_3(\varphi^4)$, since the 3-bubbles of the amputation $\text{inn}(\mathcal{Y})^{\hat{0}}$ are quadratic vertices. We verify that the edge and vertex sets of both $\partial\mathcal{G} \sqcup \partial\mathcal{H}$ and $\partial\mathcal{Y}$ are the same, as well as the adjacency. If \mathcal{G} and \mathcal{H} have no external edges, then the result is a trivial equality of empty graphs. Then we assume that at least one of them has external legs.

- *Vertices.* Notice that $\#$ is additive in the number of external vertices of its graph summands. Since \mathcal{P} has no external vertices, it follows from the definition of boundary graph that the number of vertices of $\partial\mathcal{Y}$ is the sum of those of $\partial\mathcal{G}$ plus those of $\partial\mathcal{H}$. Thus, both vertex-sets of graphs in both sides of (27) are identical, also with the same bipartiteness.
- *Edges.* For any vertices $x, c \in \partial\mathcal{Y}$ and for any colour $a = 1, 2, 3$, we prove, that joining them, there exist an a -coloured edge f_a in the graph $\partial\mathcal{Y}$ if and only if there exists an a -coloured edge f'_a of $\partial\mathcal{G} \sqcup \partial\mathcal{H}$ between x and c . The case in which x and c are both white or both black vertices is trivial, for there is no path between them. Thus, we assume w.l.o.g. that x is black and c white and prove now both directions of the equivalence:

(\Rightarrow) If $f_a = \overline{cx} \in (\partial\mathcal{Y})_a^{(1)}$ the first thing to notice is that, referring to in Fig 5a, there is no bicolored path through $(\mathcal{P} \wedge k) \wedge l$ that joins d with q nor p with b . This means that c and x are either both in $\partial\mathcal{G}$ or both in $\partial\mathcal{H}$. The case is symmetric in \mathcal{G} and \mathcal{H} and we thus suppose the former case, $c, x \in (\partial\mathcal{G})^{(0)}$, and prove that there is a $(0a)$ -bicolored path *entirely in* $\partial\mathcal{G}$ joining them. By definition of boundary graph, there is a $(0a)$ -bicolored path γ in \mathcal{Y} between c and x , that originates the edge $f_a = \overline{cx}$. Let g' be the 0-colour edge created by the sum $g \#_k$ in \mathcal{Y} . The edge g' belongs to the subgraph $(\mathcal{P} \wedge k) \wedge l$ of \mathcal{Y} (see Fig 5a). We discern two cases:

- *Case 1:* If γ does not pass through g' . In this case, γ itself is a bicolored path in \mathcal{G} between the given vertices c and x . Thus γ also originates an a -coloured edge between these.
- *Case 2:* If γ does pass through g' . This means, as shown in Figure 5a, that for any color a , γ will pass through k' as well. But, since γ joins c with x , this means that

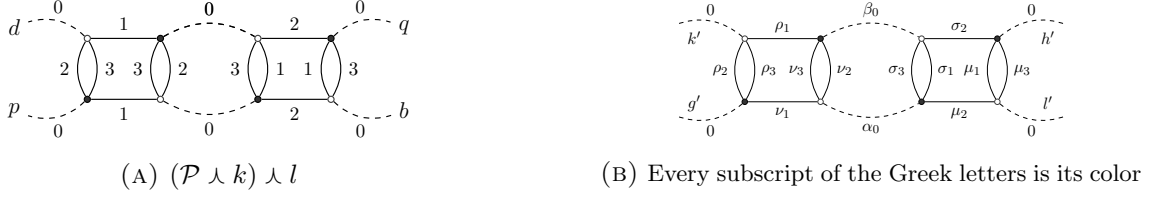


FIGURE 5. On the proof of Lemma 6

in \mathcal{G} , there is an $a0$ -bicolored path from c to x (passing through g , which differs from γ only in that edge).

This shows $\partial\mathcal{Y}_a^{(1)} \subset (\partial\mathcal{G} \sqcup \partial\mathcal{H})_a^{(1)}$ for arbitrary a .

(\Leftarrow) Assume that there exists an edge $f'_a \in (\partial\mathcal{G} \sqcup \partial\mathcal{H})_a^{(1)}$ between c and x . Then either both x, c are external vertices of \mathcal{G} or both of \mathcal{H} .

- If x, c are in $\mathcal{G}_{\text{out}}^{(0)}$. Again, f'_a is originated by certain $(a0)$ -bicolored path ζ in \mathcal{G} . If the edge g does not lie on this path, then the whole path is still in \mathcal{Y} , so $f_a \in (\partial\mathcal{Y})_a^{(1)}$. On the other hand, if g is one of the propagators in ζ , notice that the same path ζ with g replaced by the concatenation of the following edges

$$\begin{cases} g'\nu_1\alpha_0\sigma_1\beta_0\rho_1k' & \text{if } a = 1 \\ g'\rho_ak' & \text{if } a \neq 1 \end{cases}$$

is a $(0a)$ -bicolored path that lies in $(\partial\mathcal{Y})_a^{(1)}$ and goes from c to x .

- If x, c are in $\mathcal{H}_{\text{out}}^{(0)}$. Similarly, f_a is originated by certain $(a0)$ -bicolored path ξ in \mathcal{H} . If the edge h does not lie on this path, obviously $f_a \in (\partial\mathcal{Y})_a^{(1)}$. But if h is one of the 0 -colored edges in the bicolored path ξ , notice that replacing h in ξ by the concatenation of

$$\begin{cases} h'\sigma_2\beta_0\nu_2\alpha_0\mu_2l' & \text{if } a = 2 \\ h'\mu_ah' & \text{if } a \neq 2 \end{cases}$$

lies in $(\partial\mathcal{Y})_a^{(1)}$, and is a $(0a)$ -bicolored path from c to x . Thus $(\partial\mathcal{H})_a^{(1)} \subset \partial\mathcal{Y}_a^{(1)}$.

In any case, we have shown the direction $\partial\mathcal{Y}_a^{(1)} \supset (\partial\mathcal{G} \sqcup \partial\mathcal{H})_a^{(1)}$ and thus the lemma as well. □

We use this result to prove the main result of this section. Before doing so, we need another result. For any non-negative integer g , let $\Sigma^g = \#^g\mathbb{T}^2$ (this $\#$ is the usual topological connected sum. Also $\Sigma^0 = \mathbb{S}^2$).

Lemma 7. *For each $g \in \mathbb{Z}_{\geq 0}$ there exists a φ_3^4 -Feynman graph \mathcal{T}_g whose boundary graph $\partial\mathcal{T}_g$ triangulates Σ^g .*

Proof. We define the following (so-called canonical [9]) 3-colored graphs \mathcal{C}_g of genus g . For $g = 0$, \mathcal{C}_0 is just the graph Θ . For $g \in \mathbb{Z}_{>0}$, one now constructs \mathcal{C}_g form a regular $2(2g + 1)$ -agon whose vertices are colorated in an alternating way: black, white, black, white, ...; between those, the sides are given also an alternating edge-coloration $(1, 2, 1, 2, \dots)$. To this $2(2g + 1)$ -agon we add its $(2g + 1)$ longest diagonals and color these edges with 3. The resulting graph is \mathcal{C}_g (for instance, \mathcal{C}_1 is $K_c(3, 3)$). The terminology ‘genus’ for these graphs is appropriate. Indeed, \mathcal{C}_g has $2(2g + 1)$ vertices, $3(2g + 1)$ edges and 3 two-bubbles (faces) it is a ribbon graph that can be drawn on a surface of maximal Euler characteristic $3 - (3 - 2) \cdot (2g + 1) = 2 - 2g$, or minimal genus g .

The next step in the proof is to construct, for each genus g , a graph $\mathcal{T}_g \in \mathfrak{Feyn}_3(\varphi^4)$ with $\partial\mathcal{T}_g = \mathcal{C}_g$. This graph is constructed in two stages. First, in the vertex-set $\mathcal{C}_g^{(0)}$, one replaces

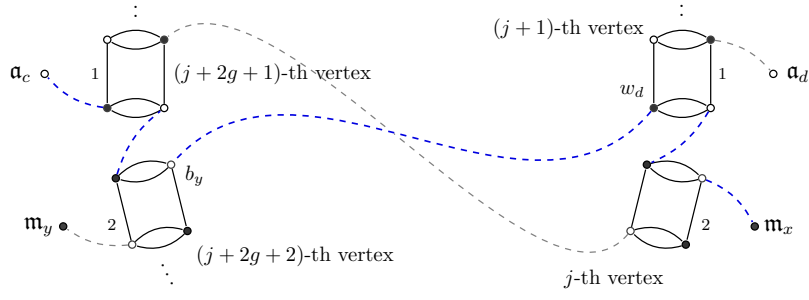


FIGURE 6. If there is a 3-colored edge $e \in \mathcal{C}_g$ one contracts $w_{s(e)}$ and $b_{t(e)}$. When one does this for all the 3-colored edges, one guarantees that, given two vertices, c and x joined by a 3-colored edge in \mathcal{C}_g , there is a propagator between w_d and b_y , where d comes after to x and y comes after c , anticlockwise. The (03)-colored path between the external vertices of \mathbf{a}_c and \mathbf{m}_x passes through $\overline{w_d b_y}$.

any black vertex x and any white vertex c by the following rule:



The second stage is to contract with propagators in order to obtain a well defined element of $\mathfrak{Fenn}_3(\varphi^4)$. For each 1 colored line \overline{cx} in \mathcal{C}_g (if it exists) we join o_c and p_x with a propagator. If there is a 2-colored edge \overline{cx} in \mathcal{C}_g , one joins d_c with q_x with a propagator. It is immediate to see that adjacency by an a -colored edge \overline{cx} in \mathcal{C}_g leads to connectivity between \mathbf{a}_c and \mathbf{m}_x by a $(0a)$ -bicolored path, for $a = 1, 2$. We want the same property for $a = 3$, and actually, for each 3-colored line between the given vertices x and c , one joins w_c and b_x with a propagator. Remarkably this does *not* imply the (03)-path connectedness between c and x but that of their succeeding vertices of the $2(2g+1)$ -gon. Thus, said connectivity between a 3-colored edge \overline{cx} is provided by a path composed of nine edges passing through a propagator between w_d and b_y , where d (resp. y) is the white (resp. black) vertex in the polygon, succeeding c (resp. x), as shown in Figure 6. The graph assembled by applying these two steps to each vertex and edge of \mathcal{C}_g is called \mathcal{T}_g and, by construction, it satisfies $\partial\mathcal{T}_g = \mathcal{C}_g$. This proves the result. \square

Some \mathcal{C}_g for higher genera are depicted in Fig. 7. As example of this construction, \mathcal{T}_1 is the leftmost graph in eq. (17). The more complex \mathcal{T}_4 is shown in Figure 7c. We observe that the set $\mathbf{T} = \{\mathcal{T}_0, \mathcal{T}_1, \mathcal{T}_2, \dots\} \subset \mathfrak{Fenn}_3(\varphi^4)$ endowed with the contraction $\#$ is a monoid and the restriction $(\Delta \circ \partial)|_{\mathbf{T}}$ to that set is a monoid-morphism $(\mathbf{T}, \#) \rightarrow (\text{Riem}_{c,cl,o}, \#)$.

Theorem 8. *The map θ defined by*

$$\theta = \Delta \circ \partial : \mathfrak{Fenn}_3(\varphi^4) \xrightarrow{\partial} \text{IIGrph}_{\text{col},3} \xrightarrow{\Delta} \text{Riem}_{\text{cl},o}$$

is surjective. That is, all closed, orientable (possibly disconnected) Riemannian surfaces are cobordant via a manifold triangulated by (connected graphs of) the φ_3^4 -theory.

Proof. If M has b boundary components, there are b (not necessarily different) integers $g_1, \dots, g_b \in \mathbb{Z}_{\geq 0}$ such that

$$M \simeq \Sigma^{g_1} \sqcup \Sigma^{g_2} \sqcup \dots \sqcup \Sigma^{g_b}. \quad (28)$$

We construct a graph $\mathcal{L}_{g_1, \dots, g_b} \in \mathfrak{Fenn}_3(\varphi^4)$ with $\Delta(\partial\mathcal{L})$ homeomorphic to M . We consider the following sum:

$$\mathcal{L}_{g_1, \dots, g_b} := (\mathcal{T}_{g_1})_{f_1} \#_k \mathcal{P}_l \#_{e_2} (\mathcal{T}_{g_2})_{f_2} \#_k \mathcal{P} \dots \mathcal{P}_l \#_{e_b} (\mathcal{T}_{g_b}).$$

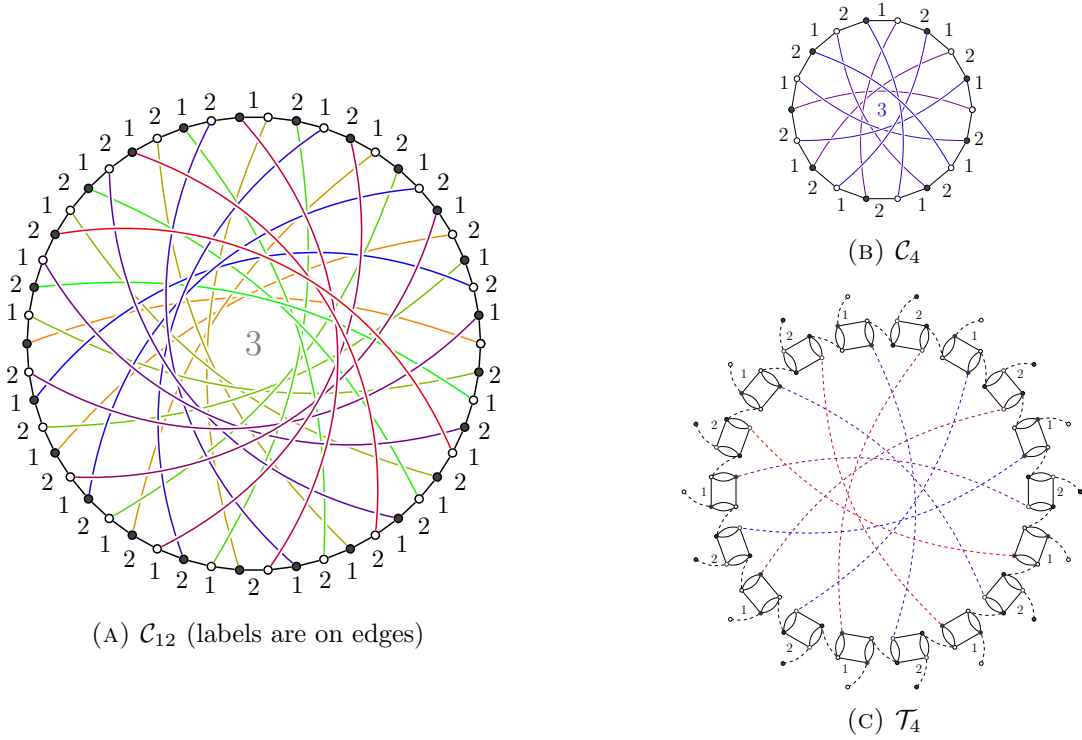


FIGURE 7. Examples of canonical graphs \mathcal{C}_g , for $g = 4$, based on an octadecagon, and for $g = 12$ on a pentacontagon (a). The graph in (c) satisfies $\partial\mathcal{T}_4 = \mathcal{C}_4$; see Lemma 7 (colors in the online version only as visual guide).

Notice that each \mathcal{T}_{g_i} has more than three internal propagators and we choose two arbitrary 0-colored edges e_i, f_i of \mathcal{T}_{g_i} to perform the connected sum. Because all its summands are in $\mathfrak{Feyn}_3(\varphi^4)$, so is $\mathcal{L}_{g_1, \dots, g_b}$. We suppress the edge dependence. Finally, $\mathcal{L}_{g_1, \dots, g_b}$ satisfies

$$\begin{aligned} \partial\mathcal{L}_{g_1, \dots, g_b} &= \partial((\mathcal{T}_{g_1})\#\mathcal{P}\#(\mathcal{T}_{g_2})\#\mathcal{P}\dots\mathcal{P}\#(\mathcal{T}_{g_b})) = \partial(\mathcal{T}_{g_1}) \sqcup \partial((\mathcal{T}_{g_2})\#\mathcal{P}\dots\mathcal{P}\#(\mathcal{T}_{g_b})) = \dots \\ &= \partial(\mathcal{T}_{g_1}) \sqcup \dots \sqcup \partial(\mathcal{T}_{g_b}) = \mathcal{C}_{g_1} \sqcup \dots \sqcup \mathcal{C}_{g_b}, \end{aligned}$$

by applying $b - 1$ times Lemma 6 and b times Lemma 7. Thus $\theta(\mathcal{L}_{g_1, \dots, g_b}) = \Delta(\partial\mathcal{L}_{g_1, \dots, g_b}) \simeq M$, which proves the theorem. \square

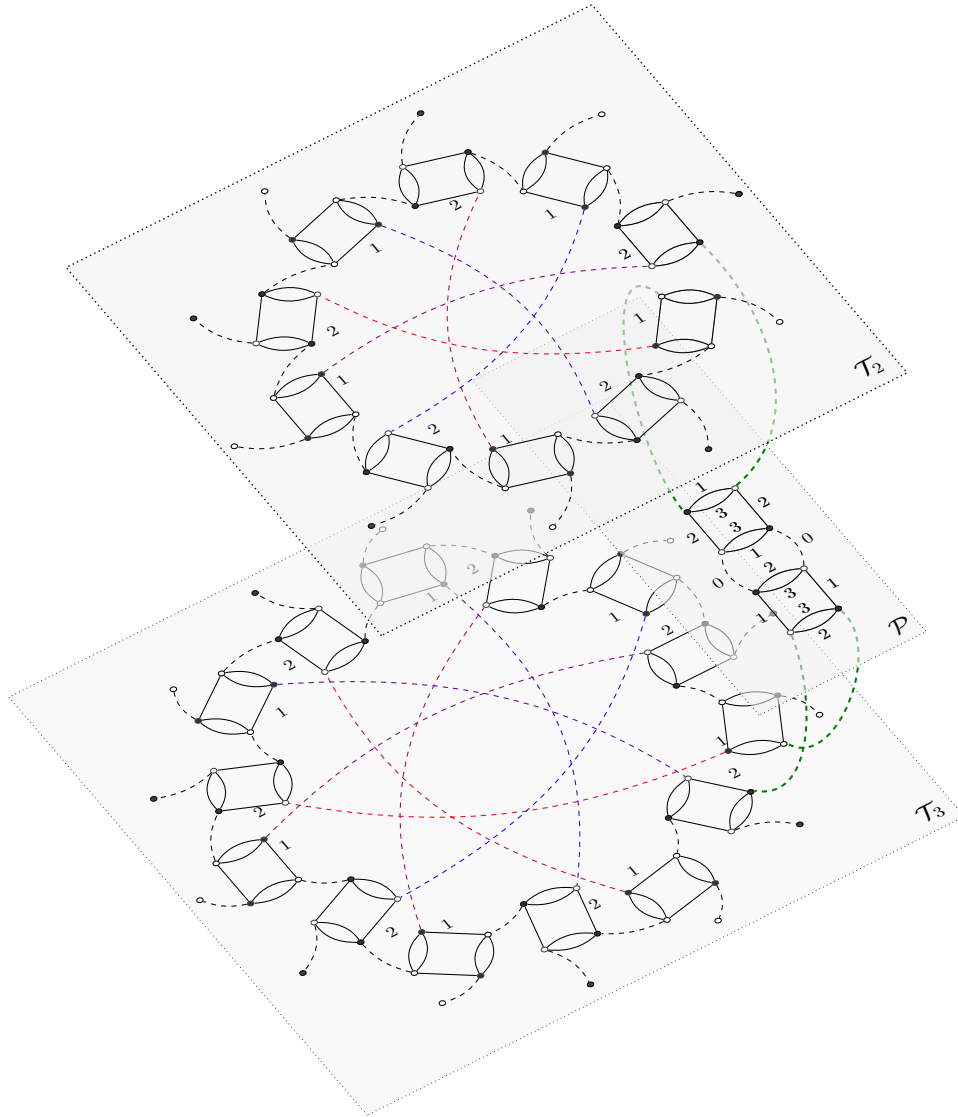
As example of how this construction works, a bordism $\Sigma^2 \rightarrow \Sigma^3$ is shown in Figure 8.

5. CONCLUSIONS

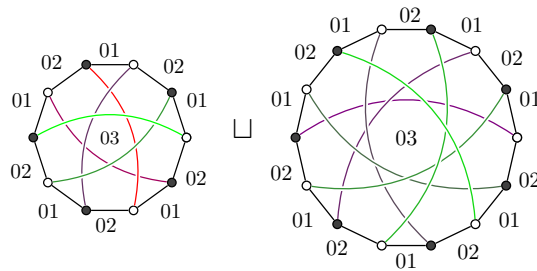
We defined the connected sum of 3-colored graphs that is a well defined operation on the set of Feynman diagrams of any tensor model. It differs from the existent connected sum in the crystallization theory by a 1-dipole move. There is no tensor model V such that the latter operation restricts to a well defined binary operation on $\mathfrak{Feyn}_2(V)$, whence the need of the connected sum we introduced. It is used to prove the surjectivity of the map ξ in the following commuting diagram:

$$\begin{array}{ccc} & \mathfrak{Feyn}_2((\varphi\bar{\varphi})^2) & \\ \swarrow & & \searrow \xi \\ \cup_{k=0}^{\infty} \text{Grph}_{\text{col}, 2+1}^{(2k)} & \xrightarrow{\Delta} & 2\text{-Cob} \end{array} \quad (29)$$

(see Thm. 5). Tangentially, this might provide some link between the rank-2 tensor models and Atiyah's Topological Quantum Field Theories [2], where one studies functors from 2-Cob to the category of Hilbert spaces. A particular case of (29) is $\xi|$ in the following commutative



(A) The graph $\mathcal{L}_{2,3}$



(B) The graph $\partial\mathcal{L}_{2,3} = \mathcal{C}_2 \sqcup \mathcal{C}_3$

FIGURE 8. Example of a bordism $\Sigma^2 \rightarrow \Sigma^3$ triangulated by a Feynman graph $\mathcal{L}_{2,3}$ of the φ_3^4 -theory, as given in the proof of Theorem 8 (coloring of the lines in the on line version only intended as visual guide).

diagram:

$$\begin{array}{ccc}
 & \mathfrak{Feyn}_2^v((\varphi\bar{\varphi})^2) & \\
 \swarrow & & \searrow \xi| \\
 \text{Grph}_{\text{col},2+1} & \xrightarrow{\Delta} & \text{Riem}_{\text{c},\text{cl},\text{o}}
 \end{array} \tag{30}$$

Trivially, CTM-graphs that represent a (sub)category of boundaryless manifolds (here $\text{Riem}_{c,\text{cl},o}$) can be exhibited as null-bordant, by just coning each graph. The non trivial part is showing that, in this case, any surface in $\text{Riem}_{c,\text{cl},o}$ is null-bordant via a suitable graph in $\mathfrak{Feyn}_3(\varphi^4)$, which we constructed. Moreover, any two surfaces in $\text{Riem}_{\text{cl},o}$ (even disconnected) are also cobordant in the sense of the φ_3^4 -theory:

$$\begin{array}{ccc}
 & \mathfrak{Feyn}_3(\varphi^4) & \\
 \partial \swarrow & & \searrow \theta \\
 \text{IIGrph}_{\text{col},3} & \xrightarrow{\Delta} & \text{Riem}_{\text{cl},o}
 \end{array} \tag{31}$$

An immediate consequence concerns the non-perturbative [35] treatment of the Ward Identity for rank-3 tensor models [34, 40]. In order to undertake that problem, one needs the expansion of the free energy $\log Z[J, \bar{J}]$ in boundary graphs, analogous to in the matrix model case [20, Sec. 2.3]. The fact that the boundary sector $\partial\mathfrak{Feyn}_3(\varphi^4)$, as proven here, generates all of $\text{Riem}_{\text{cl},o}$ facilitates our Ansatz regarding this expansion.

The divergence degree of graphs can be expressed in terms of certain degree $\tilde{\omega}$ for open graphs, that extends Gurău's degree ω . The degree for open graphs is given in terms of the so called pinched jackets of \mathcal{G} . For us, it is important that the genus and Gurău's degree are the same for 3-colored graphs. One has then for an open Feynman graph \mathcal{G} , $\tilde{\omega}(\mathcal{G}) \geq 3 \cdot \omega(\partial\mathcal{G}) = 3 \sum_{\mathcal{R} \subset \partial\mathcal{G}} g(\mathcal{R})$, summing⁸ over the the connected components of the boundary graph $\partial\mathcal{G}$. The present work helps to compute the boundary graph $\partial\mathcal{G}$, and hence to have a lower-bound for the degree $\tilde{\omega}(\mathcal{G})$.

In [35] it will be proven that the correlation functions $G_{\mathcal{B}}$ of the φ_3^4 -model are indexed by boundary graphs $\mathcal{B} \in \partial\mathfrak{Feyn}_3(\varphi^4)$. It will be useful to expand these functions in Gurău's degree, as done in the matrix theory-formulation of the ($\Omega = 1$)-Grosse-Wulkenhaar φ^4 -model [20] in terms of the genus. In there, using such expansion, combined with the a full Ward identity and the Schwinger-Dyson equations yielded a closed equations for correlation functions and that techniques will be extended to the present setting.

As another immediate application, the natural continuation of this work is to relax some of the symmetry and to pose Question (\star) in the framework of multi-orientable [43] or $O(N)$ -tensor models [12].

A second, quite different application is the addition of bosonic fields. In dimension two, for instance, using Theorem 5 and constructs before it, one has control of the gluings' topology, even of those made of a large number of interaction vertices. This can both ease computations and might be reused to define gauge theories on (computable) random spaces. An approach is, first, to adapt the gauge theory on usual graphs à la Baez [3] to our colored graphs. Secondly, one would add gauge fields à la Marcolli-van Suijlekom [28] using representation of graphs (here tensor-model Feynman graphs used as random-'manifold base') in the category of finite dimensional spectral triples with vanishing Dirac operator. In that respect, the connection between noncommutative geometry and matrix models would be based on recent results by Barrett and Glaser [4], which treat the *quantum* Connes-Chamseddine spectral action [13, 14] as a certain matrix model.

ACKNOWLEDGEMENT

The author wishes to thank:

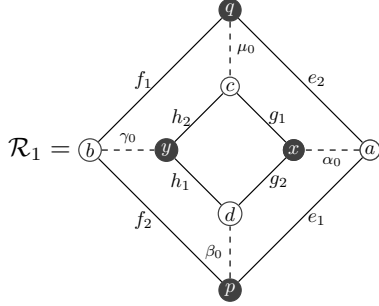
- The *Deutscher Akademischer Austauschdienst* (DAAD) mainly, but also the *Sonderforschungsbereich 878* "Groups, Geometry & Actions" (SFB 878), for financial support.
- Paola Cristofori, Joseph Ben Geloun, Raimar Wulkenhaar for useful comments and Adrian Tanasă for pointing out the multi-orientable tensor models.

⁸The inequality has been proven in [6, Lemma 4] (see also [41, Cor. B4]); for the equality, see here Example 2.

- The Erwin Schrödinger International Institute for Mathematical Physics, Vienna, for hospitality during the ESI-Program “The interrelation between mathematical physics, number theory and non-commutative geometry”.

APPENDIX A. COMPUTING HOMOLOGY OF COLORED GRAPHS

Example 9. To compute its bubble-homology, as proposed in Ex. 2 one chooses an (ordered) basis for each dimension according to following labels:



$$\begin{aligned} C_0(\mathcal{R}_1) &= \langle a, b, c, d, p, q, x, y \rangle_{\mathbb{Z}}, \\ C_1(\mathcal{R}_1) &= \langle e_1, e_2, f_1, f_2, g_1, g_2, h_1, h_2, \alpha_0, \beta_0, \gamma_0, \mu_0 \rangle_{\mathbb{Z}}, \\ C_2(\mathcal{R}_1) &= \langle \mathcal{B}^{01}, \mathcal{B}^{02}, \mathcal{B}_{\text{outside}}^{12}, \mathcal{B}_{\text{inside}}^{12} \rangle_{\mathbb{Z}}. \end{aligned}$$

In the chain complex $0 \rightarrow \mathbb{Z}^4 \simeq C_2(\mathcal{R}_1) \xrightarrow{\partial_2} \mathbb{Z}^{12} \simeq C_1(\mathcal{R}_1) \xrightarrow{\partial_1} C_0(\mathcal{R}_1) \simeq \mathbb{Z}^8 \rightarrow 0$ the non-trivial boundary operators are, in the chosen bases, given by:

$$\partial_1 = \begin{pmatrix} -1 & -1 & 0 & 0 & 0 & 0 & 0 & 0 & 0 & -1 & 0 & 0 & 0 \\ 0 & 0 & -1 & -1 & 0 & 0 & 0 & 0 & 0 & 0 & -1 & 0 & 0 \\ 0 & 0 & 0 & 0 & -1 & 0 & 0 & -1 & 0 & 0 & 0 & -1 & 0 \\ 0 & 0 & 0 & 0 & 0 & 0 & -1 & -1 & 0 & 0 & -1 & 0 & 0 \\ 1 & 0 & 0 & 0 & 1 & 0 & 0 & 0 & 0 & 0 & 1 & 0 & 0 \\ 0 & 0 & 1 & 1 & 0 & 0 & 0 & 0 & 0 & 0 & 0 & 0 & 1 \\ 0 & 0 & 0 & 0 & 0 & 1 & 1 & 0 & 0 & 1 & 0 & 0 & 0 \\ 0 & 0 & 0 & 0 & 0 & 0 & 0 & 1 & 1 & 0 & 0 & 1 & 0 \end{pmatrix} \sim \begin{pmatrix} 1 & 0 & 0 & 1 & 0 & 0 & 0 & 0 & 0 & 1 & 0 & 0 & 0 \\ 0 & 1 & 0 & -1 & 0 & 0 & 0 & 0 & 0 & 0 & -1 & 0 & 1 \\ 0 & 0 & 1 & 1 & 0 & 0 & 0 & 0 & 0 & 0 & 1 & 0 & 0 \\ 0 & 0 & 0 & 1 & 0 & 0 & 1 & 0 & 0 & 0 & 0 & 0 & 1 \\ 0 & 0 & 0 & 0 & 1 & 0 & -1 & 0 & 1 & -1 & 0 & 0 & 0 \\ 0 & 0 & 0 & 0 & 0 & 1 & 1 & 0 & 0 & 1 & 0 & 1 & 0 \\ 0 & 0 & 0 & 0 & 0 & 0 & 0 & 1 & -1 & 1 & -1 & 1 & -1 \\ 0 & 0 & 0 & 0 & 0 & 0 & 0 & 0 & 0 & 0 & 0 & 0 & 0 \end{pmatrix}$$

and

$$\partial_2 = \begin{pmatrix} 1 & 0 & -1 & 0 \\ 0 & 1 & 1 & 0 \\ 1 & 0 & -1 & 0 \\ 0 & 1 & 1 & 0 \\ 1 & 0 & 0 & -1 \\ 0 & 1 & 0 & 1 \\ 1 & 0 & 0 & -1 \\ 0 & 1 & 0 & 1 \\ -1 & -1 & 0 & 0 \\ -1 & -1 & 0 & 0 \\ -1 & -1 & 0 & 0 \\ -1 & -1 & 0 & 0 \end{pmatrix} \sim \begin{pmatrix} 1 & 0 & 0 & 0 \\ 0 & 1 & 0 & 0 \\ 1 & 0 & 0 & 0 \\ 0 & 1 & 0 & 0 \\ 0 & 0 & 1 & 0 \\ 1 & 1 & -1 & 0 \\ 0 & 0 & 1 & 0 \\ 1 & 1 & -1 & 0 \\ -1 & -1 & 0 & 0 \\ -1 & -1 & 0 & 0 \\ -1 & -1 & 0 & 0 \\ -1 & -1 & 0 & 0 \end{pmatrix},$$

where the tilde means a change of basis, which in each case leads to row or column reduction. Since $\partial_3 = 0$, $H_2(\mathcal{R}_1) = \ker \partial_2 = \mathbb{Z}$. On the other hand the column reduction of ∂_1 is

$$\partial_1 M = \begin{pmatrix} 1 & 0 & 0 & 0 & 0 & 0 & 0 & 0 & 0 & 0 & 0 & 0 & 0 \\ 0 & 1 & 0 & 0 & 0 & 0 & 0 & 0 & 0 & 0 & 0 & 0 & 0 \\ 0 & 0 & 1 & 0 & 0 & 0 & 0 & 0 & 0 & 0 & 0 & 0 & 0 \\ 0 & 0 & 0 & 1 & 0 & 0 & 0 & 0 & 0 & 0 & 0 & 0 & 0 \\ 0 & 0 & 0 & 0 & 1 & 0 & 0 & 0 & 0 & 0 & 0 & 0 & 0 \\ 0 & 0 & 0 & 0 & 0 & 1 & 0 & 0 & 0 & 0 & 0 & 0 & 0 \\ 0 & 0 & 0 & 0 & 0 & 0 & 1 & 0 & 0 & 0 & 0 & 0 & 0 \\ -1 & -1 & -1 & -1 & -1 & -1 & -1 & -1 & 0 & 0 & 0 & 0 & 0 \end{pmatrix}$$

where

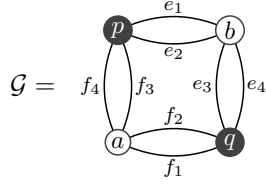
$$M = \begin{pmatrix} 0 & 0 & 0 & 0 & 1 & 0 & 0 & 0 & -1 & -1 & 0 & 0 \\ 0 & 1 & 0 & 0 & 0 & 1 & 0 & 0 & 1 & 0 & 1 & -1 \\ 0 & -1 & 0 & 0 & 0 & 0 & 0 & 0 & -1 & 0 & -1 & 0 \\ 0 & 0 & 0 & 0 & 0 & 0 & 0 & 0 & 1 & 0 & 0 & 0 \\ 0 & 0 & -1 & 0 & 0 & 0 & 0 & -1 & 0 & 0 & 0 & -1 \\ 1 & 1 & 1 & 0 & 1 & 1 & 1 & 1 & 0 & -1 & 1 & 0 \\ -1 & -1 & -1 & -1 & -1 & -1 & -1 & -1 & 0 & 0 & -1 & 0 \\ 0 & 0 & 0 & 0 & 0 & 0 & 0 & 0 & 1 & 0 & 0 & 0 \\ -1 & -1 & 0 & 0 & -1 & -1 & 0 & 0 & 0 & 1 & -1 & 1 \\ 0 & 0 & 0 & 0 & 0 & 0 & 0 & 0 & 0 & 1 & 0 & 0 \\ 0 & 0 & 0 & 0 & 0 & 0 & 0 & 0 & 0 & 1 & 0 & 0 \\ 0 & 0 & 0 & 0 & 0 & 0 & 0 & 0 & 0 & 0 & 1 & 0 \end{pmatrix}. \text{ Then } M^{-1}\partial_2 = \begin{pmatrix} 0 & 0 & 0 & 0 \\ 0 & 0 & 0 & 0 \\ 0 & 0 & 0 & 0 \\ 0 & 0 & 0 & 0 \\ 0 & 0 & 0 & 0 \\ 0 & 1 & 0 & 1 \\ 0 & 1 & 1 & 0 \\ -1 & -1 & 0 & 0 \\ -1 & -1 & 0 & 0 \\ -1 & -1 & 0 & 0 \end{pmatrix}$$

The last zero-columns of ∂_1 correspond to the generators of $\ker \partial_1 = \mathbb{Z}^5$. From those generators, which in the matrix $M^{-1}\partial_2$ correspond to the five last rows, three of them —the non-zero rows corresponding to the row reduction of the (non-zero lower part of $M^{-1}\partial_2$)

$$\begin{pmatrix} 1 & 0 & 0 & -1 \\ 0 & 1 & 0 & 1 \\ 0 & 0 & 1 & -1 \\ 0 & 0 & 0 & 0 \\ 0 & 0 & 0 & 0 \end{pmatrix}$$

—lie also in the image of ∂_2 . It follows $H_1(\mathcal{R}_1) = \mathbb{Z}^5 / \mathbb{Z}^3 = \mathbb{Z}^2$.

Example 10. In order to compute the homology of the the complex, one labels the graph



$$\begin{aligned} C_0(\mathcal{G}) &= \langle a, p, b, q \rangle_{\mathbb{Z}} \\ C_1(\mathcal{G}) &= \langle e_1, e_2, e_3, e_4, f_1, f_2, f_3, f_4 \rangle_{\mathbb{Z}} \\ C_2(\mathcal{G}) &= \langle \mathcal{B}_e^{12}, \mathcal{B}_f^{12}, \mathcal{B}^{23}, \mathcal{B}^{24}, \mathcal{B}^{13}, \mathcal{B}^{14}, \mathcal{B}_e^{34}, \mathcal{B}_f^{34} \rangle_{\mathbb{Z}} \\ C_3(\mathcal{G}) &= \langle \mathcal{B}^1, \mathcal{B}^2, \mathcal{B}^3, \mathcal{B}^4 \rangle_{\mathbb{Z}} \end{aligned}$$

where \mathcal{B}^c means omission of the color c . The differentials of the chain complex

$$0 \rightarrow C_3(\mathcal{G}) \simeq \mathbb{Z}^4 \xrightarrow{\partial_3} C_2(\mathcal{G}) \simeq \mathbb{Z}^8 \xrightarrow{\partial_2} C_1(\mathcal{G}) \simeq \mathbb{Z}^8 \xrightarrow{\partial_1} C_0(\mathcal{G}) \simeq \mathbb{Z}^4 \rightarrow 0$$

are explicitly:

$$\partial_1 = \begin{pmatrix} 0 & 0 & -1 & -1 & -1 & -1 & 0 & 0 \\ 1 & 1 & 1 & 1 & 0 & 0 & 0 & 0 \\ -1 & -1 & 0 & 0 & 0 & 0 & -1 & -1 \\ 0 & 0 & 0 & 0 & 1 & 1 & 1 & 1 \end{pmatrix}, \quad \partial_2 = \begin{pmatrix} -1 & 0 & 0 & 0 & -1 & -1 & 0 & 0 \\ 1 & 0 & -1 & -1 & 0 & 0 & 0 & 0 \\ 0 & 0 & 1 & 0 & 1 & 0 & -1 & 0 \\ 0 & 0 & 0 & 1 & 0 & 1 & 1 & 0 \\ 0 & -1 & 0 & 0 & -1 & -1 & 0 & 0 \\ 0 & 1 & -1 & -1 & 0 & 0 & 0 & 0 \\ 0 & 0 & 1 & 0 & 1 & 0 & 0 & -1 \\ 0 & 0 & 0 & 1 & 0 & 1 & 0 & 1 \end{pmatrix}, \quad \partial_3 = \begin{pmatrix} 0 & 0 & 1 & 1 \\ 0 & 0 & 1 & 1 \\ 1 & 0 & 0 & 1 \\ -1 & 0 & 1 & 0 \\ 0 & 1 & 0 & -1 \\ 0 & -1 & -1 & 0 \\ 1 & 1 & 0 & 0 \\ 1 & 1 & 0 & 0 \end{pmatrix}$$

To compute H_2 , the reduced versions are

$$\partial'_2 = \begin{pmatrix} 1 & 0 & 0 & 0 & 0 & 0 & 0 & 0 \\ 0 & 1 & 0 & 0 & 0 & 0 & 0 & 0 \\ 0 & 0 & 1 & 0 & 0 & 0 & 0 & 0 \\ -1 & -1 & -1 & 0 & 0 & 0 & 0 & 0 \\ 0 & 0 & 0 & 1 & 0 & 0 & 0 & 0 \\ 1 & 1 & 0 & -1 & 0 & 0 & 0 & 0 \\ 0 & 0 & 0 & 0 & 1 & 0 & 0 & 0 \\ -1 & -1 & 0 & 0 & -1 & 0 & 0 & 0 \end{pmatrix}, \quad \partial'_3 = \begin{pmatrix} 0 & 0 & 0 & 0 \\ 0 & 0 & 0 & 0 \\ 0 & 0 & 0 & 0 \\ 0 & 0 & 0 & 0 \\ 0 & -1 & -1 & 0 \\ 0 & 1 & 0 & -1 \\ 1 & 1 & 0 & 0 \end{pmatrix} \sim \begin{pmatrix} 0 & 0 & 0 & 0 \\ 0 & 0 & 0 & 0 \\ 0 & 0 & 0 & 0 \\ 0 & 0 & 0 & 0 \\ 1 & 0 & 0 & 1 \\ 0 & 1 & 0 & -1 \\ 0 & 0 & 1 & 1 \end{pmatrix}$$

The non-zero part of ∂'_3 has rank three, whence $H_2(\mathcal{G}) = \mathbb{Z}^3/\mathbb{Z}^3 = 0$. Similarly one finds $H_1(\mathcal{G}) = 0$.

APPENDIX B. THE CELL COMPLEX OF A RIBBON GRAPH

Departing from the abstract definition, we construct here the cell-decomposition of the minimum-genus-surface where a ribbon graph can be drawn on without self-intersections. To begin with, we remark that vertices do not have naturally an orientation, but only a cyclic order—so far, these are only abstract combinatorial objects. However, when one tries to represent graphs by drawings, thus evoking the orientation of the plane (counterclockwise), graphs might be given a neater representation if we invert the cyclic order on some vertices and, of course, keep track of this action with help of a sign, ϵ . Write $\epsilon_v = +1$ if we preserve the order of a vertex v as the levorotation, and $\epsilon_v = -1$ if the cyclic order of v is written as a dextrorotary vertex. Also, for any ribbon graph \mathcal{R} , since each edge e is determined by two half-edges $h, h' \in \mathcal{R}^{(1/2)}$ that are joined (i.e. $j(h) = h'$), e can be rewritten as $e = [h, h'] = [h', h]$. If $e = [(v, \alpha), (w, \beta)]$, think of e as being attached to the vertex v at the α -th place, and to the vertex w in the β -th place.

The ‘fat graph’ representation of \mathcal{R} is in a natural way a cell-complex, $X(\mathcal{R})$. The skeleta $X^{(n)}$ are constructed as follows:

0-cells: Let n_v be the valence of the vertex $v \in \mathcal{R}^{(0)}$, and $\epsilon_v \in \{+1, -1\}$ its orientation. We associate v the following cyclic ordered set (see Fig. 9) of 0-cells:

$$v \rightarrow \begin{cases} (P(v)_1^+, P(v)_1^-, P(v)_2^+, P(v)_2^-, \dots, P(v)_{n_v}^+, P(v)_{n_v}^-) & \text{if } \epsilon_v = +1, \\ (P(v)_1^+, P(v)_1^-, P(v)_{n_v}^+, P(v)_{n_v}^-, \dots, P(v)_2^+, P(v)_2^-) & \text{if } \epsilon_v = -1. \end{cases} \quad (32)$$

The 0-skeleton $X^{(0)}$ is then the union of all such points $P(v)_\alpha^\epsilon$, with v running all over $\mathcal{R}^{(0)}$, $\epsilon = \pm$ and $\alpha = 1, \dots, n_v$. One has thus, in total, $2 \sum_{v \in \mathcal{R}^{(0)}} n_v$ 0-cells.

1-cells: In order to construct $X^{(1)}$, we proceed in two steps:

i) First, add a 1-cell \overline{pq} to for each consecutive pair of points p and q , with the order given by the cycles (32). That is, add for each vertex v the following cells:

$$\overline{P(v)_1^+ P(v)_1^-}, \overline{P(v)_1^- P(v)_2^+}, \dots, \overline{P(v)_{n_v}^+ P(v)_{n_v}^-}, \overline{P(v)_{n_v}^- P(v)_1^+} \quad (\epsilon_v = +1) \quad (33)$$

$$\overline{P(v)_1^+ P(v)_1^-}, \overline{P(v)_1^- P(v)_{n_v}^+}, \dots, \overline{P(v)_2^+ P(v)_2^-}, \overline{P(v)_2^- P(v)_1^+} \quad (\epsilon_v = -1) \quad (34)$$

This results in the space $\sqcup_{v \in \mathcal{R}^{(0)}} (\mathbb{S}_v^1)^\pm$, where the circles is given the orientation \pm of the vertices.



(A) For a positively orientable vertex $(v, +) \in \mathcal{R}^{(0)}$, with $n_v = 6$.

(B) For a, say, valence-4 vertex, the associated 0-cells.

FIGURE 9. On the construction of the 0-skeleton, $X^{(0)}$ of \mathcal{R} .

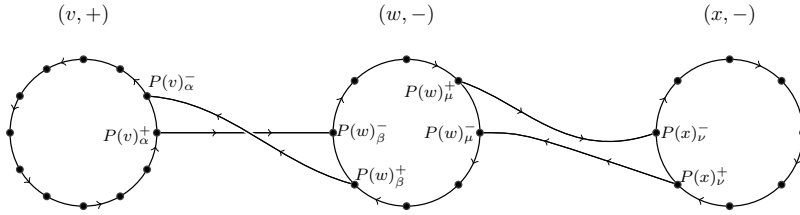


FIGURE 10. Shows the most general case on how to adjoin 1-cells. First, to the cyclic structure in eq. (32) (in the figure, the circles). Here the 1-cells attached to an edge e that connects with $e = [(v, \alpha), (w, \beta)]$; the opposite orientation is responsible for the apparent crossing. On the right, the two 1-cells associated to $f \in \mathcal{R}^{(1)}$, if $f = [(w, \mu), (x, \nu)]$.

- ii) The second step is attaching the ribbons: for each edge $e \in \mathcal{R}^{(1)}$ with $e = [(x, \alpha), (y, \beta)]$ (viz. connecting the vertex x at the α -th place, with y at the β -th place), attach 1-cells from $P(x)_\alpha^+$ to $P(y)_\beta^-$ and from $P(y)_\beta^+$ to $P(x)_\alpha^-$ (see Fig. 1 (B) and Fig. 10). Notice that the same edges are attached if we instead take the pair $((y, \beta), (x, \alpha))$ as representative. Since for each vertex v we attached double lines, the whole number of attached 1-cells is $2 \sum_{v \in \mathcal{R}^{(0)}} n_v + 2|\mathcal{R}^{(1)}|$.

2-cells. The last skeleton $X^{(2)}$ is obtained in two steps:

- filling the ribbon double lines: that is, if $e \in \mathcal{R}^{(1)}$ and $e = [(v, \alpha), (w, \beta)]$, 2-disk attachment at the loop formed by $\overline{P(v)_\alpha^+ P(v)_\alpha^-}$, $\overline{P(w)_\beta^+ P(w)_\beta^-}$ and the two ribbon segments constructed for e in step ii) above.
- The second step is filling for all $v \in \mathcal{R}^{(0)}$ the vertex-circles \mathbb{S}_v^1 which one gets by (33). In total, we added $|\mathcal{R}^{(1)}| + |\mathcal{R}^{(0)}|$ 2-cells.

This exhibits the cell-structure $X^{(2)}$ of a ribbon graph. But actually is more natural not to stop at $X^{(2)}$ and to adjoin more 2-cells to some loops left, namely the boundary components. A *boundary component* of the graph \mathcal{R} here is a loop of the graph formed by the boundary of the ribbons' long segments and arcs determined by the orientation, as pictured in Figure 11 (A) (see also Fig. 1 (B)).

Formally, these boundary components are described as follows: take an arbitrary edge $e = [(v, \alpha), (w, \beta)]$ and let $s(\alpha)$ be the next place according to the cyclic ordering given to v (i.e. $s(\alpha) \equiv \alpha \pm 1 \pmod{n_v}$ if $\epsilon_v = \pm$). Thus, consider the path that begins with the segments $\overline{P(w)_\beta^+ P(v)_\alpha^-}$, $\overline{P(v)_\alpha^- P(v)_{s(\alpha)}^+}$. We can juxtapose another segment, since there is a unique $f \in \mathcal{R}^{(1)}$ and a unique $x \in \mathcal{R}^{(0)}$ with $f = [(v, s(\alpha)), (x, \gamma)]$. The process finishes after a finite number of steps by coming back to $P(w)_\beta^+$, at the latest, when we run out of vertices. The loop ℓ_1 obtained by concatenation of these paths (see Fig. 11 (B))

$$\ell_1 = \overline{P(w)_\beta^+ P(v)_\alpha^- P(v)_{s(\alpha)}^+ P(x)_\gamma^- \dots P(w)_\beta^+}$$

is a boundary component. It might be that the not all vertices lie on ℓ_1 , so pick one such a vertex and repeat the process to get ℓ_2 . The final number of non-intersecting loops—that is, after each 0-cell $p \in X^{(0)}$

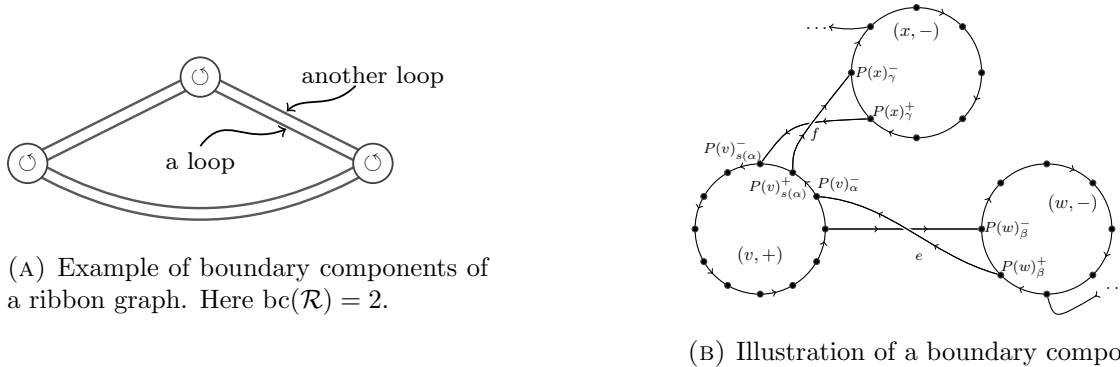


FIGURE 11. On the definition of boundary components.

lies precisely in one of the $\ell_1, \ell_2, \dots, \ell_{\text{bc}(\mathcal{R})}$ — defines $\text{bc}(\mathcal{R})$, the *number of boundary components*.

Thus each boundary component ℓ is, by construction, homeomorphic to \mathbb{S}_ℓ^1 by certain map, say φ_ℓ . Then we attach to the ribbon picture $X^{(2)}$ a 2-cell \mathring{D}_ℓ^2 by such a map $\varphi_\ell : \partial \mathring{D}_\ell^2 \rightarrow \mathbb{S}_\ell^1$, for each $\ell = 1, \dots, \text{bc}(\mathcal{R})$. The cell-structure of $\Sigma(\mathcal{R})$ is that of \mathcal{R} but with $\text{bc}(\mathcal{R})$ more 2-cells. Thus

$$\begin{aligned} |0\text{-cells of } \Sigma(\mathcal{R})| &= 2 \sum_{v \in \mathcal{R}^{(0)}} n_v, \\ |1\text{-cells of } \Sigma(\mathcal{R})| &= 2 \sum_{v \in \mathcal{R}^{(0)}} n_v + 2|\mathcal{R}^{(1)}|, \\ |2\text{-cells of } \Sigma(\mathcal{R})| &= |\mathcal{R}^{(0)}| + |\mathcal{R}^{(1)}| + \text{bc}(\mathcal{R}). \end{aligned}$$

Since we have a finite cell-complex, we conclude from this:

$$\chi(\Sigma(\mathcal{R})) = \sum_j (-1)^j |j\text{-cells of } \Sigma(\mathcal{R})| = |\mathcal{R}^{(0)}| - |\mathcal{R}^{(1)}| + \text{bc}(\mathcal{R}).$$

Since \mathcal{R} has been assigned a cell-structure as well, ‘ $\chi(\mathcal{R})$ ’ is now misleading. It will *not* denote $\chi(X(\mathcal{R}))$ but $\chi(\Sigma(\mathcal{R}))$, as in stated in Definition 9.

Remark 6. Notice that, by construction, the inclusion of the cell-complex into a closed, compact surface $\Sigma(\mathcal{R})$ is an embedding $X(\mathcal{R}) \hookrightarrow \Sigma(\mathcal{R})$.

The next result is nothing unexpected. It shows that the two definitions of Euler characteristic harmonically coexist:

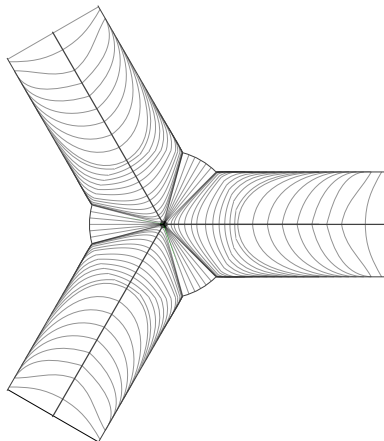
Proposition 9. *The Euler characteristic of a 3-colored graph is the same, either if we compute it by its bubble homology or, by appealing its ribbon graph structure, via its geometric realization.*

Proof. Let \mathcal{G} be a 3-colored graph. Because of Lemma 1, we can consider the cell complex $X(\mathcal{G})$ embedded in the ribbon graph realization $\Sigma(\mathcal{G})$. We transform $\Sigma(\mathcal{G})$ into another cell-complex $Y(\mathcal{G})$ by a deformation retraction. We retract the ribbons’ disks to thin edges and the vertices’ disks to actual point-like vertices; see Fig. 12 (A). We end up with

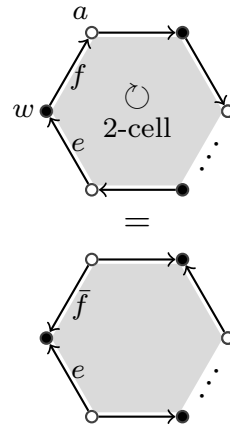
$$|0\text{-cells}| = |\mathcal{G}^{(0)}|, \quad |1\text{-cells}| = |\mathcal{G}^{(1)}|, \quad |2\text{-cells}| = \text{bc}(\mathcal{G}).$$

We claim that the complex associated to $Y(\mathcal{G})$ is the same cell-complex obtained by bubble homology.

For cells of dimensions $p = 0, 1$, the statement is trivially verified, since a graph is, naturally, a cell-complex. For dimension 2, we observe that each boundary component we attached 2-cells to, was formed by arcs on the disks, and segments on the next edge (determined by the cyclic ordering at the vertex). After the deformation retraction, the arcs no longer exist. Therefore the boundary component is now composed by the 1-cells determined by only the edges as follows. Pick a boundary component and an arbitrary edge e lying on it. Let c be the color of e . Then pick the black vertex (name it w) e is attached to. The next edge f has then color $c - 1 \pmod{3}$, since w has orientation (321). By the same token, f is attached to a white vertex, say a , that determines the next edge lying on the boundary component; this has color c again, for a has been assigned the orientation (123). This yields then a sequence of edges that forms connected path of edges of alternating colors $\{c, c - 1\}$. Thus, each one of the attached 2-cells to the boundary components of $X(\mathcal{G})$ corresponds, after the deformation retraction, to a bicolored connected path. These are, by definition, 2-bubbles. Therefore $C_2(Y(\mathcal{G})) = C_2(\mathcal{G})$.



(A) The deformation retraction $\Sigma(\mathcal{G}) \rightarrow Y(\mathcal{G})$ in local coordinates on a neighborhood of a vertex. The disk is continuously collapsed to a point-like vertex, and the ribbons sent to the (1-dimensional) half-edges as shown.



(B) On the two different orientations of edges. The first, determined by the cell-complex construction of ribbon graphs (above) and the lower one by the cell-attachment by bubble homology, see eq. (10) with $p = 2$.

FIGURE 12. On the proof of Proposition 9.

On the equivalence of the boundary operators: The boundary operator $\partial'_2 : C_2(Y(\mathcal{G})) \rightarrow C_1(Y(\mathcal{G}))$ is the sum of all edges that lie on a boundary component, with ‘compatible orientation’ (that is, if the edges e and f meet at the vertex w , then f and e point in opposite directions, as seen from w). Since any generator of $C_2(Y(\mathcal{G}))$ is of the form $\mathcal{B}^{(ij)}$, with $i < j$,

$$\begin{aligned} \partial'_2(\mathcal{B}^{(ij)}) &= \sum_{\text{all edges, } e_c \subset \mathcal{B}^{(ij)}} e_c = \sum_{e \in \mathcal{G}_i^{(1)}} e + \sum_{f \in \mathcal{G}_j^{(1)}} f \\ &= \sum_{e \in \mathcal{G}_i^{(1)}} e - \sum_{f \in \mathcal{G}_j^{(1)}} \bar{f} = \partial_2(\mathcal{B}^{(ij)}). \end{aligned}$$

where \bar{f} is the edge with the opposite orientation (cf. Fig. 12 (B)). □

REFERENCES

- [1] Jan Ambjørn, Bergfinnur Durhuus, and Thordur Jonsson. Three-dimensional simplicial quantum gravity and generalized matrix models. *Mod. Phys. Lett.*, A6:1133–1146, 1991.
- [2] M. Atiyah. Topological quantum field theories. *Inst. Hautes Etudes Sci. Publ. Math.*, 68:175–186, 1989.
- [3] John C. Baez. Spin network states in gauge theory. *Adv. Math.*, 117:253–272, 1996. arXiv:gr-qc/9411007.
- [4] John W. Barrett and Lisa Glaser. Monte Carlo simulations of random non-commutative geometries. *J. Phys.*, A49(24):245001, 2016. arXiv:1510.01377.
- [5] Joseph Ben Geloun and Vincent Rivasseau. A Renormalizable 4-Dimensional Tensor Field Theory. *Commun. Math. Phys.*, 318:69–109, 2013. arXiv:1111.4997.
- [6] Joseph Ben Geloun and Dine Ousmane Samary. 3D Tensor Field Theory: Renormalization and One-loop β -functions. *Annales Henri Poincaré*, 14:1599–1642, 2013. arXiv:1201.0176.
- [7] Valentin Bonzom, Răzvan Gurău, Aldo Riello, and Vincent Rivasseau. Critical behavior of colored tensor models in the large N limit. *Nucl. Phys.*, B853:174–195, 2011. arXiv:1105.3122.
- [8] Valentin Bonzom, Răzvan Gurău, and Vincent Rivasseau. Random tensor models in the large N limit: Uncoloring the colored tensor models. *Phys. Rev.*, D85:084037, 2012. arXiv:1202.3637.
- [9] Sylvain Carrozza. *Tensorial methods and renormalization in Group Field Theories*. PhD thesis, Orsay, LPT, 2013.
- [10] Sylvain Carrozza. Flowing in group field theory space: a review. *SIGMA*, 2016. arXiv:1603.01902.
- [11] Sylvain Carrozza, Daniele Oriti, and Vincent Rivasseau. Renormalization of a SU(2) Tensorial Group Field Theory in Three Dimensions. *Commun. Math. Phys.*, 330:581–637, 2014. arXiv:1303.6772.
- [12] Sylvain Carrozza and Adrian Tanasa. $O(N)$ Random Tensor Models. *Lett. Math. Phys.*, 106(11):1531–1559, 2016. arXiv:1512.06718.
- [13] Ali H. Chamseddine and Alain Connes. The Spectral action principle. *Commun. Math. Phys.*, 186:731–750, 1997.

- [14] Ali H. Chamseddine, Alain Connes, and Matilde Marcolli. Gravity and the standard model with neutrino mixing. *Adv. Theor. Math. Phys.*, 11(6):991–1089, 2007.
- [15] P. Di Francesco. Rectangular matrix models and combinatorics of colored graphs. *Nucl. Phys.*, B648:461–496, 2003. arXiv:cond-mat/0208037.
- [16] P. Di Francesco, Paul H. Ginsparg, and Jean Zinn-Justin. 2-D Gravity and random matrices. *Phys. Rept.*, 254:1–133, 1995. arXiv:hep-th/9306153.
- [17] M. Ferri, C. Gagliardi, and L. Grasselli. A graph-theoretical representation of PL-manifolds — a survey on crystallizations. *Aequationes Mathematicae*, 31(1):121–141, 1986.
- [18] Laurent Freidel. Group field theory: An Overview. *Int. J. Theor. Phys.*, 44:1769–1783, 2005. arXiv:hep-th/0505016.
- [19] Joseph Ben Geloun. Renormalizable Tensor Field Theories. In *18th International Congress on Mathematical Physics (ICMP2015) Santiago de Chile, Chile, July 27-August 1, 2015*, 2016. arXiv:1601.08213.
- [20] Harald Grosse and Raimar Wulkenhaar. Self-Dual Noncommutative φ^4 -Theory in Four Dimensions is a Non-Perturbatively Solvable and Non-Trivial Quantum Field Theory. *Commun. Math. Phys.*, 329:1069–1130, 2014. arXiv:1205.0465.
- [21] Răzvan Gurău. Colored Group Field Theory. *Commun. Math. Phys.*, 304:69–93, 2011. arXiv:0907.2582.
- [22] Răzvan Gurău. The $1/N$ expansion of colored tensor models. *Annales Henri Poincaré*, 12:829–847, 2011. arXiv:1011.2726.
- [23] Răzvan Gurău. A review of the large- N limit of tensor models. *Symmetries and Groups in Contemporary Physics*, 2012. arXiv:1209.4295.
- [24] Răzvan Gurău. The complete $1/N$ expansion of colored tensor models in arbitrary dimension. *Annales Henri Poincaré*, 13:399–423, 2012. arXiv:1102.5759.
- [25] Răzvan Gurău. Universality for Random Tensors. *Ann. Inst. H. Poincaré Probab. Statist.*, 50(4):1474–1525, 2014. arXiv:1111.0519.
- [26] Răzvan Gurău and James P. Ryan. Colored Tensor Models - a review. *SIGMA*, 8:020, 2012. arXiv:1109.4812.
- [27] Thomas Krajewski and Reiko Toriumi. Exact Renormalisation Group Equations and Loop Equations for Tensor Models. *SIGMA*, 12:068, 2016.
- [28] Matilde Marcolli and Walter D. van Suijlekom. Gauge networks in noncommutative geometry. *Journal of Geometry and Physics*, 75:71 – 91, 2014. arXiv:1301.3480.
- [29] Edwin E. Moise. Affine Structures in 3-Manifolds: V. The Triangulation Theorem and Hauptvermutung. *Annals of Mathematics*, 56(1):96–114, 1952.
- [30] M. Mulase and M. Penkava. Ribbon graphs, quadratic differentials on Riemann surfaces, and algebraic curves defined over $\overline{\mathbb{Q}}$. *Asian J. Math.*, 2(4):875–919, 1998.
- [31] nLab. <https://ncatlab.org/nlab/show/ribbon+graph>.
- [32] Daniele Oriti. Group Field Theory and Loop Quantum Gravity. 2014. arXiv:1408.7112.
- [33] Dine Ousmane Samary. Beta functions of $U(1)^d$ gauge invariant just renormalizable tensor models. *Phys. Rev.*, D88(10):105003, 2013. arXiv:1303.7256.
- [34] Dine Ousmane Samary, Carlos I. Pérez-Sánchez, Fabien Vignes-Tourneret, and Raimar Wulkenhaar. Correlation functions of a just renormalizable tensorial group field theory: the melonic approximation. *Class. Quant. Grav.*, 32(17):175012, 2015. arXiv:1411.7213.
- [35] Carlos I. Pérez-Sánchez. The full Ward-Takahashi Identity for colored tensor models. 2016. arXiv:1608.08134.
- [36] Mario Pezzana. Sulla struttura topologica delle varietà compatte. *Ati Sem. Mat. Fis. Univ. Modena*, 23(1):269–277, 1975.
- [37] Vincent Rivasseau. The Tensor Theory Space. *Fortsch. Phys.*, 62:835–840, 2014. arXiv:1407.0284.
- [38] Vincent Rivasseau. Random Tensors and Quantum Gravity. *SIGMA*, 12:069, 2016. arXiv:1603.07278.
- [39] James P. Ryan. Tensor models and embedded Riemann surfaces. *Phys. Rev.*, D85:024010, 2012. arXiv:1104.5471.
- [40] Dine Ousmane Samary. Closed equations of the two-point functions for tensorial group field theory. *Class. Quant. Grav.*, 31:185005, 2014. arXiv:1401.2096.
- [41] Dine Ousmane Samary and Fabien Vignes-Tourneret. Just Renormalizable TGFT’s on $U(1)^d$ with Gauge Invariance. *Commun. Math. Phys.*, 329:545–578, 2014. arXiv:1211.2618.
- [42] Adrian Tanasă. Multi-orientable Group Field Theory. *J. Phys.*, A45:165401, 2012. arXiv:1109.0694.
- [43] Adrian Tanasă. The Multi-Orientable Random Tensor Model, a Review. *SIGMA*, 12:056, 2016.